

# On Topology of Perturbed Vortices

Taosif Ahsan,<sup>1</sup> S.A. Cohen,<sup>2</sup> and A.H. Glasser<sup>3</sup>

<sup>1</sup>*Plasma Science and Fusion Center, Massachusetts Institute of Technology, Cambridge MA 02179*

<sup>2</sup>*Princeton Plasma Physics Laboratory, Princeton University, Princeton, NJ, 08543 USA*

<sup>3</sup>*Fusion Theory and Computation, Inc., 24062 Seatter Lane NE, Kingston, WA 98346*

(Dated: February 3, 2026)

This work shows that the interiors of perturbed zero-helicity vortices display simply connected topology with a crescent-shaped boundary. Flux surfaces in fluid and magnetic vortices were explored analytically, while particle trajectories in the context of plasma confinement were examined numerically, demonstrating the existence of both toroidal and simply connected topologies. This new topology appears for perturbations in a broad class, with amplitudes and spatial variance allowed to be arbitrarily small. A corollary of this work proves the closedness of field lines under odd-parity perturbations of zero-helicity vortices in full three dimensional context.

## I. INTRODUCTION

To improve the confinement of plasma, many magnetic-confinement fusion-reactor (MFE) designs have a toroidal topology, *e.g.*, tokamaks, stellarators, reversed-field pinches, and spheromaks. In the spheromak category there is a promising type of fusion confinement device, with spacecraft propulsion applications, called the field-reversed configuration (FRC) [1–3] sustained by adding an odd-parity rotating magnetic field (RMF) to Hill’s vortex like background magnetic field structure [4–6]. The FRC-RMF system can be modeled as a perturbed zero-helicity structure such as Soloviev equilibrium [7] and, equivalently, Hill’s vortex [6, 8]. These vortices have found further importance in broad and diverse fields such as accretion disks in astrophysics [9–11], geophysical dynamics [12], and even biological systems like jellyfish motion [13–15]. Given an exactly equivalent mathematical structure, the work presented in this paper equally applies to a broad array of phenomena.

This motivates a systematic analysis of zero-helicity vortex structures. Hill’s seminal 1894 paper, by solving the Euler equations, described a self-sustaining spherical vortex moving like a solid body within a fluid [8]. Wan [16] proved that Hill’s vortex is an energy-maximizing system using the variational principle. Amick and Fraenkel [17] demonstrated the uniqueness of the solution. The long-held assumption is that the topology of these vortices is toroidal, which, as this paper will show, is not necessarily true.

The topological shape of the vortices is primarily characterized by the flux surfaces, defined as level sets of flux functions. For axisymmetric vortices, the flux function forms a set of foliated tori. In fluid vortices, the field lines are equivalent to particle motion, and they thus trivially stick to the flux surfaces. In magnetic field vortices, when plasma particles remain near a particular foliation, the particle’s gyroradius is the characteristic radial step size due to Coulomb collisions, which determines confinement. Particles with small gyro radii generally follow field lines, so the topology of flux surfaces, which are a continuous and smooth collection of field lines, is vital in understanding particle confinement. In some toroidal

devices, such as tokamaks, many particle trajectories significantly deviate from a flux surface, forming drift surfaces, *e.g.*, banana orbits [18]. Confinement is severely degraded because the characteristic step size increases to the banana width. Zero-helicity structures, such as FRCs, have mostly been treated as toroidal inside their bounding surface, the separatrix. The existence of non-toroidal flux surfaces may have implications for plasma confinement and stability.

Several studies have examined axisymmetric perturbed vortices [19–21], and numerical studies have been conducted on three-dimensional perturbations of Hill’s vortices [4, 22]. Axially non-symmetric perturbations have significant consequences for plasma confinement. Reference [23] showed that an even-parity perturbation fully opens up closed field lines of toroidal plasma devices, predicting degraded plasma confinement, much to the despair of FRC enthusiasts. (In this paper and [4, 23, 24], parity of the perturbation is understood to be parity with respect to the plane  $z$ .)

Nevertheless, additional discoveries significantly improved hope for plasma confinement using RMF-induced FRC systems. A preliminary version of the work in this paper was done in [4, 24]. Firstly, the resilience of field-line closure under odd-parity perturbation was observed in simulations done in [4]. But conjecture based on simulation is not always valid, and rigorous analysis is preferable in understanding the total picture.

Given the topological nature of the conjecture, static analysis is sufficient for the study. [24] attempted to analytically prove the observations and partially succeeded in proving the closure by developing an mathematical object named modified flux function (MFF). [24] also found the exact range of perturbation magnitude that preserves closure. However, the analysis was done for a limited two-dimensional slab of the full three-dimensional system. The analytical justification behind the conjectures postulated in [4] in a real-life three-dimensional context remained elusive, significantly limiting the understanding of the system.

This paper attempts to finally resolve this limitation using tools from differential topology. It has succeeded

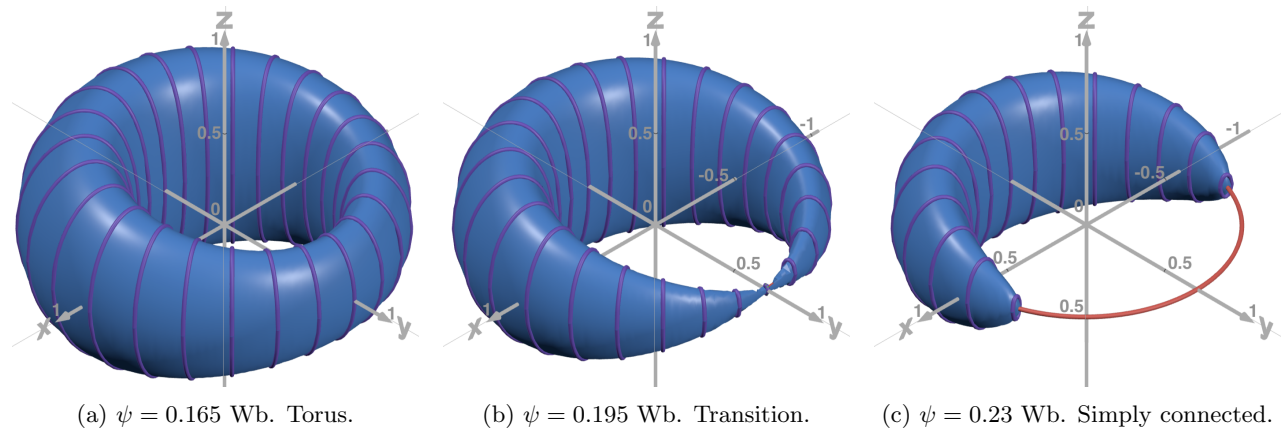


FIG. 1: The flux surfaces (blue) and field lines (purple) transition from toroidal to simply connected as  $\psi$  increases. The red circle is the ‘O’-point null line on which the critical points  $\mathbf{r}_c$ , defined by  $\mathbf{B}(\mathbf{r}_c) = 0$ , lie. In (a), there is no intersection between the flux surface and the red circle; in (b), there is one intersection; and in (c), there are two intersections. Here,  $\alpha = 0.2$ ,  $k = 0.25 \text{ m}^{-1}$ ,  $B_0 = 2 \text{ T}$ ,  $r_s = z_s = 1 \text{ m}$ .

in proving the validity of the conjectures made in [4] in a full three-dimensional context. Furthermore, this analysis elucidated a more coherent picture of topological categorization beyond just closed and open field lines. An unexpected and curious result was proven: *even under infinitesimal perturbations, simply connected flux surfaces exist within zero-helicity vortices*. This was missed by the simulations and partial analysis done in [4, 24] due to lack of access to the total picture. Given that the RMF-FRC system is rather equivalent to a wide class of perturbed Hill’s vortices, the conclusion should appear in many different contexts, as noted earlier. This paper also finds physical interpretation of the modified flux function found in [24].

The paper is also interested in real particle motion beyond somewhat abstract field lines. In the context of fluid mechanics, the field lines under study are equivalent to fluid velocity fields, and the conclusions apply directly to actual particle motion. However, in the case of Hill’s vortex created from magnetic field lines used in plasma confinement, the situation is more complicated. Generally, particle motion can be approximated to first order (in the ion-cyclotron radii/system size expansion) by helical motion around a magnetic field line. But in the context of FRCs, the field goes to zero and this approximation breaks down. Thus, we wanted to push the study further and investigate whether these simply connected topologies appear in the case of particle motion as well. The numerical calculations of particle motion in Soloviev equilibria also surprisingly demonstrated the simply connected topology. Even for very small gyro-radii, particle trajectories may, counterintuitively, strongly deviate from flux surfaces, forming a volume with a simply connected boundary.

Thus, this paper has three primary advancements: it finds the full proof of the conjecture in [4], discovers new simply connected topology in Hill’s vortices, and numer-

ically shows the existence of simply connected topology in particle motion in perturbed field-reversed configurations.

## II. MODELING THE PERTURBED VORTEX WITH MODIFIED FLUX FUNCTION

In cylindrical coordinates,  $(r, \phi, z)$ , the vector field of an axisymmetric zero-helicity vortex, *e.g.*, the magnetic field of an FRC, may be represented analytically by the Soloviev equilibrium or Hill’s vortex:

$$\mathbf{B}_0 = B_0 \left( \frac{rz}{z_s^2}, 0, 1 - \frac{2r^2}{r_s^2} - \frac{z^2}{z_s^2} \right), \quad (1)$$

$$\psi_0 = \frac{B_0 r^2}{2} \left( 1 - \frac{r^2}{r_s^2} - \frac{z^2}{z_s^2} \right). \quad (2)$$

$\mathbf{B}$  can describe magnetic fields for plasma confinement or velocity fields in fluids, depending on context.  $B_0$  is the vector field strength scaling. Without perturbation, the flux function  $\psi_0$  and azimuthal angle between  $r$  and cartesian  $y$  axis,  $\phi$ , uniquely label field lines. We perturb the vortex by  $\mathbf{B} = \mathbf{B}_0 + \delta\mathbf{B}$ ,

$$\delta\mathbf{B} = -\alpha B_0 (kz \cos \phi, -kz \sin \phi, kr \cos \phi), \quad (3)$$

where  $\alpha > 0$  is a free parameter controlling the perturbation’s field strength.  $k > 0$  is the axial wavenumber of the perturbation. The ratio of the field strength of a perturbation to the vortex field is  $\sim \alpha k(r_s + z_s)$ . Despite a simple form, the perturbation model is rather general and includes any slowly spatially varying vacuum field perturbation that does not destroy closure. A detailed discussion of perturbation model is added in appendix C.

The model for unperturbed vortex did not assume any drop in electric current/vorticity outside of separatrix. This is mathematically valid but physically unsound.

The topological analysis, however, still remains physically valid because the error in physical system this assumption is second order. This can be self consistently ignored. See appendix D for more detailed rigorous discussion on this.

With the addition of an odd-parity perturbation, the previous unique labeling fails because the system is no longer axisymmetric. A unique labeling for every field line, a modified flux function (MFF), is still possible, as shown in [24]. A brief derivation of modified flux function can be found if we translate the coordinate  $\mathbf{r} \rightarrow \mathbf{r} - \alpha k z_s^2 \hat{y}$ . In this coordinate, the cylindrical radius and cylindrical coordinate azimuthal angle shift to

$$r \rightarrow \rho = \sqrt{(y - \alpha k z_s^2)^2 + x^2}, \quad (4)$$

$$\phi \rightarrow \varphi = \cot^{-1} \left( \frac{y - \alpha k z_s^2}{x} \right). \quad (5)$$

As shown in appendix A, this makes azimuthal component  $B_\varphi = 0$  and gives us a set of Clebsch coordinate,

$$\mathbf{B} = \nabla\psi \times \nabla\varphi \quad (6)$$

The significance of the Clebsch pair  $(\psi, \varphi)$  is that they are invariant along the flow and *potentially* help uniquely label connected field lines. One such set of field lines is shown in Fig. 2(c), where we have plotted level sets (flux surfaces) of  $\psi$  in  $\varphi = 0$  (or  $y - z$ ) plane. The other physical interpretation of  $\psi$  can be found by showing

$$\psi = \frac{d\Phi}{d\varphi} = \int_0^\rho B_z \rho' d\rho' \quad (7)$$

where  $d\Phi$  is the total flux flowing through the infinitesimal arc situated between  $[\varphi, \varphi + d\varphi]$  with radius  $\rho$ . The final physical interpretation of  $\psi$  is given by magnetic vector potential  $\mathbf{A} = (\psi/\rho) \hat{\varphi}$ , upto gauge. Hence we see that, even though modified flux function was first derived as a mathematical tool in [24], it has multiple grounded physical interpretation.

Using Eq. (7), one can re-derive the form of  $\psi$  found in [24]. In cartesian coordinates  $(x, y, z)$ , where  $x = r \sin \phi$ ,  $y = r \cos \phi$ ,  $z = z$ ,  $\psi$  can be written in the same form from [24],

$$\psi = \frac{B_0 r_s^2}{2} \cdot \mathbf{u}^2 (J - \mathbf{v}^2) \quad (8)$$

$$\text{where, } \mathbf{u} = \left( \frac{x}{r_s}, \frac{y - \alpha k z_s^2}{r_s}, 0 \right), \quad (9)$$

$$\mathbf{v} = \left( \frac{x}{r_s}, \frac{y}{r_s} + \frac{\alpha k r_s}{3} \left( \frac{z_s^2}{r_s^2} + 1 \right), \frac{z}{z_s} \right), \quad (10)$$

$$\text{and } J = 1 - \left( \frac{\alpha k r_s}{3} \right)^2 \left( \frac{z_s^2}{r_s^2} + 1 \right) \left( \frac{2z_s^2}{r_s^2} - 1 \right). \quad (11)$$

See appendix A for details of the calculations done to derive  $\psi$  and its physical interpretation.

### III. TOPOLOGICAL CLASSIFICATIONS

An important topological parameter from [24] is

$$\alpha_c = \frac{1}{k z_s \sqrt{1 + \frac{2z_s^2}{r_s^2}}}. \quad (12)$$

Work in [24] shows that at  $\alpha = \alpha_c$ , field lines in the  $y-z$  plane undergo a phase transition and a new non-smooth separatrix forms. However, for  $\alpha \geq \alpha_c$ , flux surfaces and field lines with the same  $\psi$  become disconnected. This ruins the possibility of unique labeling for connected lines and surfaces, along with introducing considerably more complicated topology. We therefore limit our work to  $0 < \alpha < \alpha_c$ , a reasonable assumption for small perturbations.

#### A. Observation

We note a curious observation. In Fig. 1,  $\psi$  is increased while  $\alpha < \alpha_c$  is kept fixed. We see that the flux surfaces start from a torus-like shape in Fig. 1(a), and at a critical value of  $\psi$ , the torus develops a sharp cusp (see Fig. 1(b)). Afterwards, the surface becomes simply connected (see Fig. 1(c)). From the literature, we expect a transition from open to closed flux surfaces (or field lines) at  $\psi = 0$ . Here, however, we observe a new and distinct transition between different kinds of closed flux surfaces. We are interested in understanding the mechanism behind this transition and in numerically determining when it occurs.

#### B. Definitions

In order to do this, we define the following:

$$\psi_\pm \equiv \psi(0, y_\mp, 0), \quad y_\pm = \frac{-\alpha k r_s^2 \pm r_s \sqrt{\alpha^2 k^2 r_s^2 + 8}}{4} \quad (13)$$

$$\text{Inner separatrix, } S_{in} \equiv \{\mathbf{r} : \psi(\mathbf{r}) = \psi_-\} \quad (14)$$

$$\text{Outer separatrix, } S_{out} \equiv \{\mathbf{r} : \mathbf{v}(\mathbf{r})^2 = J\} \quad (15)$$

The physical definitions of  $y = y_\pm$  are the two isolated maxima of  $\psi(0, y, 0)$ , with  $y = \alpha k z_s^2$  being the minimum; see Fig. 2(a).  $\psi_\mp = \psi(0, y_\pm, 0)$  can thus be physically understood as the two local maximum values. In both cases of  $\psi_\pm$  and  $y_\mp$ , the + subscript was chosen to indicate the larger value and the - the smaller value. These maxima are shown clearly in Fig. 2(a), where the diamonds indicate critical points.

#### C. Visualization

The intersection with the  $y - z$  plane is shown in Fig. 2(b), which is equivalent to the field lines themselves embedded on the  $y - z$  surface. The intersection of the  $\psi$  flux surfaces with the  $x - y$  plane is shown in Fig. 2(c), which

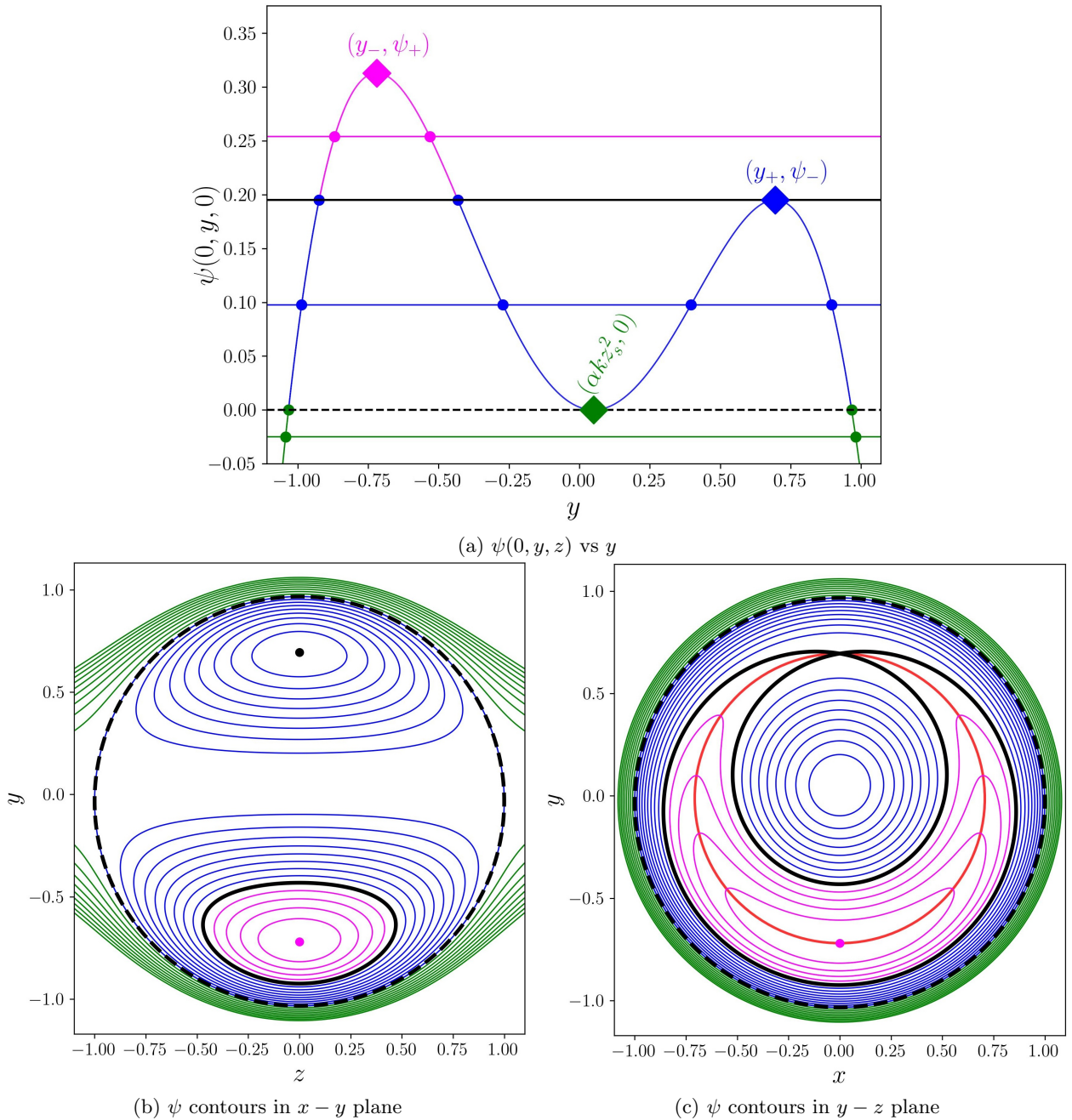


FIG. 2: (a) shows the 1-dimensional  $\psi(0, y, 0)$   $y$  plot, with diamonds indicating the critical points. (b) and (c) are 2-dimensional plot of flux surfaces intersecting with  $y - z$  and  $x - y$  planes respectively. In all figures, green, blue and magenta indicates open, torus and simply connected topology respectively. The dashed black and solid black lines indicate outer and inner separatrix respectively. (b) directly shows field lines embedded on  $y - z$  plane, while (c) can also be interpreted as Poincaré map of field lines on  $x - y$  plane. The red circle is the  $\mathbf{B} = 0$  critical point circle in (c). Here,  $\psi \in [-0.2, \psi_+ = 0.313]$  Wb,  $\alpha = 0.2$ ,  $k = 0.25 \text{ m}^{-1}$ ,  $B_0 = 2 \text{ T}$ ,  $r_s = z_s = 1 \text{ m}$ .

is equivalent to the Poincaré map of field lines. In all figures, we use green for the  $\psi \in (-\infty, 0)$  range, blue for the  $\psi \in (0, \psi_-)$  range, and magenta for the  $\psi \in (\psi_-, \psi_+]$  range. We also use a dashed black line for  $\psi = 0$  and a solid black line for  $\psi = \psi_-$ .

In Fig. 2(a), as  $\psi = \text{const.}$  is increased from negative

values (green section) to  $\psi = 0$ , the number of intersections with  $\psi(0, y, 0)$  increases from 2 to 3. Afterwards, the blue  $\psi = \text{const.}$  lines intersect  $\psi(0, y, 0)$  four times. This indicates a potential topological transition. Indeed, in Fig. 2(b) we see that this is the boundary where the system transitions from open lines and surfaces (green)

to closed lines and surfaces, hence it is named the outer separatrix  $S_{out}$  and is shown as the dashed black line in Fig. 2(a).

The second important event occurs when  $\psi$  is increased from the blue region to  $\psi_-$ , where the number of intersections in Fig. 2(a) again drops to 3. Afterwards, in the magenta section, the number of intersections drops to 2. This indicates another potential topological transition at  $\psi = \psi_-$ . However, we observe no topological difference between the lines on either side of the solid black line  $\psi = \psi_-$  in Fig. 2(b), and it is tempting to conclude that no topological transition occurs, as was concluded in [24]. However, we note that the solid black line level set has an extra isolated point on the upper side of the  $y$  axis. Fig. 2(c) is revealing: the magenta flux surfaces inside the crescent-like solid black boundary are all connected curves, while the blue flux surfaces outside all have two disconnected halves. This indicates that the flux surfaces are transitioning from toroidal topology to simply connected topology. We therefore denote this newly observed transition surface as the *inner separatrix*  $S_{in}$ .

The third important event occurs when  $\psi$  reaches  $\psi_+$ , which is the reference value of  $\psi$  at  $(0, y_-, 0)$ . This is the global maximum value of  $\psi$ . Beyond this point, flux surfaces cease to exist, as can be seen in Fig. 2.

#### D. Theorems

With these understandings, we can now state the following theorems to properly classify the topology of the flux surfaces and field lines.

For  $0 < \alpha < \alpha_c$ ,

1. Any pair  $(\psi, \varphi) \in (-\infty, \psi_+) \times [0, 2\pi)$  uniquely labels connected field lines via a one-to-one function.
2. For  $\psi \in (-\infty, 0)$ , all field lines and flux surfaces are open and lie fully outside  $S_{out}$ .
3. For  $\psi \in (0, \psi_-)$ , all flux surfaces and field lines are closed and lie strictly inside  $S_{out}$  but outside  $S_{in}$ . The flux surfaces are topologically toroidal.
4. For  $\psi \in (\psi_-, \psi_+)$ , all flux surfaces and field lines are closed and lie strictly inside  $S_{in}$ . The flux surfaces are topologically spherical.

#### E. Explanatory Sketch of Proof

Explaining the full mechanism behind this sudden additional transition requires a long and rigorous mathematical proof, given in appendix B. However, it is possible to understand the main cause of this transition. We provide a short, structured sketch of the proof for all of the theorems. Points 4 to 7 are the central cause behind the appearance of simply connected surfaces.

1. Points with  $\psi > 0$  lie inside the outer separatrix, while those with  $\psi < 0$  lie outside. Flux surfaces

and field lines with  $\psi > 0$  are compact and connected.

2. Connectedness of field lines with the same  $(\psi, \varphi)$  implies a one-to-one correspondence between  $(\psi, \varphi)$  pairs and connected field lines.
3. These connected field lines with  $\psi < 0$  extend to infinity, implying that the field lines and flux surfaces are open.
4. The points  $\mathbf{r}_c$ , defined by  $\mathbf{B}(\mathbf{r}_c) = 0$ , or equivalently  $\nabla\psi(\mathbf{r}_c) = 0$ , are critical points of the system that control the topology of the  $\psi$  surfaces. These points form a circle, shown as the red circle in Figs. 1(c) and 2(c).
5.  $\psi_-$ , the inner separatrix shown as solid black line in Fig. 2(c), is where flux surfaces start intersecting critical points on the circle.
6. Below  $\psi_-$ , flux surfaces (shown as blue lines 2(c)) lack critical points due to no intersection; above it (shown in magenta lines in 2(c)), they contain two ‘o’-type critical points due to intersecting the critical red circle twice.
7. Consequently, from the *Poincaré–Hopf theorem* [25, 26] (see Appendix B.2), connected and compact surfaces with  $\psi > 0$  inside the inner separatrix are simply connected (or spherical), while those outside are toroidal.
8. The maximum possible  $\psi$  is  $\psi_+$ , beyond which no flux surfaces exist.
9. Compactness and connectedness of flux surfaces imply that field lines are closed loops, as they are intersections of flux surfaces and  $\varphi$  planes.

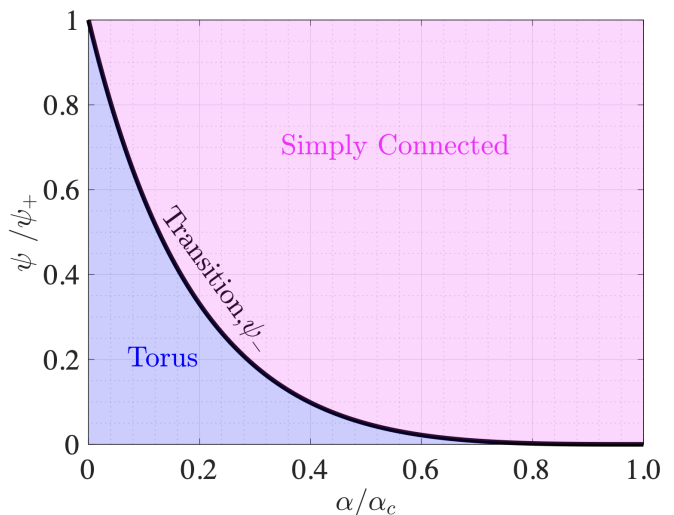


FIG. 3: Categorization of compact flux surfaces,  $0 < \psi < \psi_+$ , for all  $\alpha < \alpha_c$ . Surfaces in the blue region, magenta region, and solid black line are toroidal, simply connected, and transitional. Here  $r_s = z_s$ .

## F. Quantitative Results

$\alpha$  and  $k$  can approach zero arbitrarily closely; thus, simply connected surfaces are guaranteed to exist. For a spherical vortex ( $z_s = r_s$ ), with a small perturbation  $\alpha = 0.2\alpha_c$  or  $\alpha kr_s \approx 0.11$ , the range of  $\psi$  corresponding to compact, simply connected flux surfaces remains 67% of the total range of compact surfaces. This increases to approximately 90% at  $\alpha = 0.4\alpha_c$  or  $\alpha kr_s \approx 0.23$  and grows monotonically (see Fig. 3). Even for perturbations of this small magnitude, these ratios are not negligible, indicating that the existence is a robust feature of the Hill's vortices.

## IV. PARTICLE MOTION

In a fluid vortex, the particle/fluid motion is the same as the field lines and is guaranteed to stick to the flux surfaces discussed. Thus, particle motion has already been addressed in the previous section in the context of fluids. In the context of the  $\mathbf{B}$  representing FRC magnetic fields, particle motion deviates strongly from the field lines. The wide variety of motions can be attributed to nonlinearity such as  $\mu$  non-conservation [27]. As representative cases, we examined, *via* numerical simulation, whether electron motion exhibited simply connected patterns – closed crescent-shaped surfaces – in an FRC perturbed by static odd-parity RMF.

A parameter commonly used to demarcate between fluid-like and kinetic FRC plasmas is  $s \equiv 0.3r_s/r_g$ , where  $r_g$  is the particle gyro-radius at  $r = r_s$  and  $z = 0$ . (For  $s > 10$  the FRC is generally considered fluid; for  $s < 10$  it is generally considered kinetic.) This criterion is misleading because particles near the ‘O’-point null line or the ‘X’-point nulls experience a lower magnetic field, have larger  $r_g$ , and are in a region of greater field curvature, hence have a far lower local value  $s$ . In the simulations described below,  $s \sim 800$  but the local value of  $s$ ,  $s_l$ , may be less than 1 in places along a particle’s trajectory.

The simulations were performed with the Hamiltonian code *RMF* [28]. Typical simulations computed the trajectories of electrons with  $s = 800$ . Other relevant parameters were:  $r_s = 25$  cm,  $z_s = 75$  cm;  $B_0 = 50$  kG,  $I = 0.1 - 0.5$  (where,  $I \equiv kz_s/\pi$ ),  $\alpha = 0.01 - 0.1 \ll \alpha_c = 0.73$ , simulation duration,  $T \sim 2 - 4 \times 10^5 \tau_{ce}$  where  $\tau_{ce}$  is the period of an electron’s cyclotron motion at  $r = z = 0$ , and tolerances to numerical changes in the Hamiltonian ranged between  $10^{-8}$  and  $10^{-12}$ . The electron’s initial position was varied throughout the volume inside the (outer) separatrix. The initial velocity vector was similarly varied.  $\mu$  non-conservation decreases the average azimuthal velocity of these electrons below the thermal speed by a factor of 1000 and below the drift speed by a factor near 100. The relatively low azimuthal speed requires long-duration simulations to trace out the crescent shape.

Evident in the two cases shown in Fig. 4, the particle

trajectories show clear crescent shapes similar to the one shown in Figure 1. The orbits, in spite of the large  $s$ , are not restricted to a surface. Crescent shaped surfaces were seen up to  $I \sim 0.5$ , well beyond validity of long wave approximation.

For these long-duration simulations, the accumulated error in the Hamiltonian climbed to near 0.5% for a tolerance of  $10^{-8}$  but only to  $10^{-4}\%$  for a tolerance of  $10^{-12}$ . For this range of tolerances, occasionally the crescent tips were connected, see Figure 4 (left). Though that feature might be attributed to the Hamiltonian method not preserving phase-space structure or to the Hairy Ball Theorem, we see tip-spanning trajectories only occur at  $\mu$ -non-conserving events near the crescent tips as  $B$  approaches 0. Approximately,  $\mu$ -non-conservation occurs when  $s_l < 3$ .

That the trajectory occasionally makes azimuthal excursions close to but not precisely on the ‘O’-point null line — see the blue and green trajectory segments in Figure 4(right) — could infer that the drift surface has a toroidal geometry with the ‘O’-point line now serving as the “major axis” of the new torus and the former major axis serving as the minor axis. A rigorous criterion for the shape of these drift surfaces is under study.

Yet another difference between the drift surface crescents and those of the modified flux function is that the former are often not symmetric about the perturbation. Additionally, it should be noted that crescents with clearly separated tips have only been seen in a small percentage of simulations.

Crescent-shaped trajectory surfaces are seen both when the applied perturbation is static or rotates [6]. In the latter case, the interpretation is that charged particles are trapped in an azimuthal electric potential well. For the former, particles are trapped in a magnetic well. Depending on the direction of rotation of the perturbation, the crescents can overlay each other or be  $\pi$  radians out-of-phase.

## V. CONCLUSIONS

The modification of the flux function used in the perturbed zero helicity vortex and Soloviev equilibrium led to the discovery of simply connected flux surfaces. The classification of flux-surface topologies and field-line closure was refined *via* the calculation of an inner separatrix that separates simply connected and toroidal flux surfaces. This challenges the prevailing notion that fluid vortices and fusion confinement structures exhibit purely toroidal topology and has implications for vortex and plasma dynamics. Observations about field line closure were fully proven in three dimensional context. Simply connected topology is a robust feature in real-life stable vortices.

Numerical simulations of particle trajectories were conducted in the context of fusion confinement to calculate particle trajectories in a perturbed Soloviev equilibrium

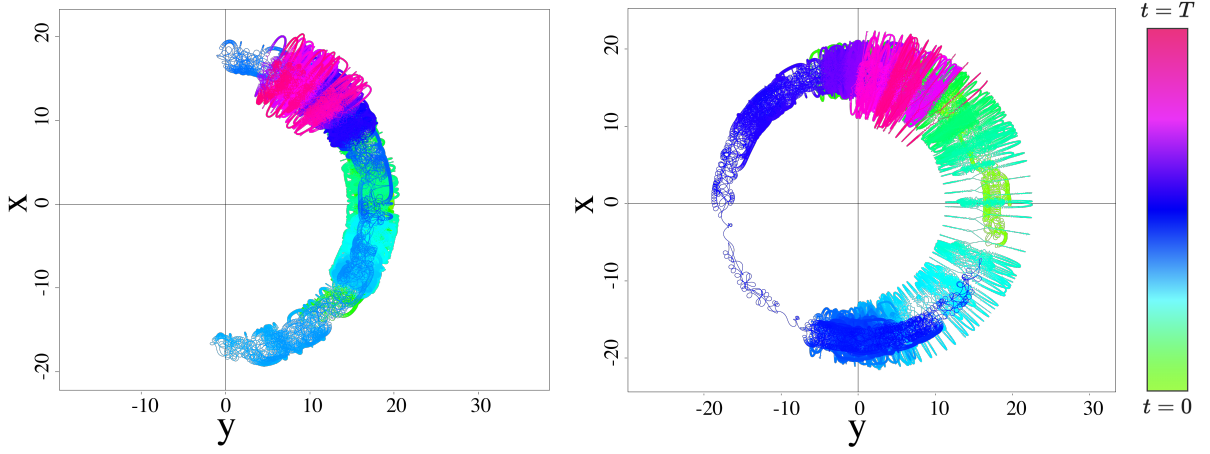


FIG. 4: Trajectories of electrons in perturbed FRC projected onto the  $x$ - $y$  plane. Unit in each axis is cm. Time is denoted by color.  $\alpha = 0.1$ ,  $I = 0.1$ ,  $r_s = 25$  cm,  $z_s = 75$  cm,  $s \sim 800$ ,  $T = 2 \times 10^5 \tau_{ce}$

where simply connected flux surfaces were observed. The orbits often displayed crescent shapes, yet showed several marked differences from the flux surfaces, *e.g.*, gyro-radii of size comparable to the crescent diameter, asymmetric crescents, connections between well-separated crescent tips, and possibly toroidal shapes, with an inversion of the roles played by the major and minor axes.

## VI. ACKNOWLEDGMENTS

The authors cordially thank Thanic Nur Samin for his valuable advice in proof. The authors also thank S. Tukachinsky and Nuno Loureiro for their comments. Support was provided, in part, by US DOE grants DE-FC02-99ER54512 and DE-AC02-09CH11466.

## VII. AUTHOR CONTRIBUTIONS

TA: Conceptualization (lead); Formal analysis (lead); Methodology (lead); Visualization (lead); Writing – original draft (lead). SAC: Simulation (lead); Conceptualization (supporting); Methodology (supporting); Project administration (lead); Writing – review and editing (supporting). AHG: Methodology (supporting); Visualization (supporting).

## Appendix A: Modified Flux Function

In cartesian coordinate, the total perturbed magnetic field is,

$$B_x = B_0 \frac{xz}{z_s^2}, \quad (\text{A1})$$

$$B_y = B_0 \frac{yz}{z_s^2}, \quad (\text{A2})$$

$$B_z = B_0 \left( 1 - \frac{2(x^2 + y^2)}{r_s^2} - \frac{z^2}{z_s^2} - \alpha ky \right), \quad (\text{A3})$$

This is not symmetric with respect to  $\phi$ . However, switching to a new cartesian coordinate with translation shift  $y' = y - \alpha k z_s^2$ , gives us an axis-symmetric system. After some calculations, we write in the new cylindrical coordinate  $(\rho, \varphi, z)$ ,

$$B_\rho = B_0 \frac{\rho z}{z_s^2}, \quad (\text{A4})$$

$$B_\varphi = 0, \quad (\text{A5})$$

$$B_z = B_0 \left( 1 - \frac{\alpha^2}{\alpha_c^2} - \frac{2\rho^2 + \alpha k(r_s^2 + 4z_s^2)}{r_s^2} \rho \cos \varphi - \frac{z^2}{z_s^2} \right) \quad (\text{A6})$$

$\rho$  and  $\varphi$  is given in Eqs. (4) and (5) and  $\alpha_c$  is given in Eq. (12). The system is still not axis-symmetric. However  $B_\varphi = 0$ . This allows us to define modified flux function such that,

$$B_\rho = -\frac{1}{\rho} \frac{\partial \psi}{\partial z}, \quad B_\varphi = 0, \quad B_z = \frac{1}{\rho} \frac{\partial \psi}{\partial \rho} \quad (\text{A7})$$

$$\implies \mathbf{B} = \nabla \psi \times \nabla \varphi \quad (\text{A8})$$

$$\implies \mathbf{B} \cdot \nabla \psi = \mathbf{B} \cdot \nabla \varphi = 0 \quad (\text{A9})$$

Which ensures that on a single field line directed by  $\mathbf{B}$  field,  $\psi$  and  $\varphi$  are invariant, and potentially can be used as a label. But there is also a physical meaning to  $\psi$  beyond just labeling,

$$d\psi = \frac{\partial \psi}{\partial \rho} d\rho + \frac{\partial \psi}{\partial \varphi} d\varphi + \frac{\partial \psi}{\partial z} dz \quad (\text{A10})$$

If we choose a path  $c$  that keeps angular and  $z$  coordinate fixed, while changing radial coordinate from 0 to  $\rho$ , we get

$$\psi = \psi(0, \varphi, z) + \int_c d\psi = \psi(0, \varphi, z) + \int_0^\rho \frac{\partial \psi}{\partial \rho'} d\rho' \quad (\text{A11})$$

We can without any loss of generality, choose  $\psi(0, \varphi, z) = 0$  and get,

$$\psi = \int_0^\rho B_z \rho' d\rho' \quad (\text{A12})$$

$$= \frac{B_0 \rho^2}{2} \left( 1 - \frac{\alpha^2}{\alpha_c^2} - \frac{\rho^2 + \frac{2}{3} \alpha k (r_s^2 + 4z_s^2) \rho \cos \varphi}{r_s^2} - \frac{z^2}{z_s^2} \right) \quad (\text{A13})$$

Shifting back to the un-shifted cartesian coordinate  $(x, y, z)$  gives for modified flux function outlined in Eqs. (8).

Total magnetic flux through an infinitesimal angular arc  $[\varphi, \varphi + d\varphi]$  with radius  $\rho$ ,

$$d\Phi = \int_\varphi^{\varphi+d\varphi} \int_0^\rho B_z \rho' d\rho' d\varphi' \quad (\text{A14})$$

$$\implies \frac{d\Phi}{d\varphi} = \psi \quad (\text{A15})$$

So, the physical interpretation of  $\psi$  is the magnetic flux going through an infinitesimal angular arc  $[\varphi, \varphi + d\varphi]$  with radius  $\rho$ . For axis-symmetric case this reduces to usual total magnetic flux through a circular surface with radius  $\rho = r$  normalized by  $2\pi$ .

There is another physical interpretation. We write the magnetic vector potential  $\mathbf{B} = \nabla \times \mathbf{A}$  in  $(\rho, \varphi, z)$  cylindrical coordinate,

$$B_\rho = \frac{1}{\rho} \frac{\partial A_z}{\partial \varphi} - \frac{\partial A_\varphi}{\partial z}, \quad (\text{A16})$$

$$B_\varphi = \frac{\partial A_\rho}{\partial z} - \frac{\partial A_z}{\partial \rho}, \quad (\text{A17})$$

$$B_z = \frac{1}{\rho} \frac{\partial(\rho A_\varphi)}{\partial \rho} - \frac{1}{\rho} \frac{\partial A_\rho}{\partial \varphi}. \quad (\text{A18})$$

We can easily match this with Eq. (A7) by choosing (upto gauge),

$$A_\rho = 0, \quad \rho A_\varphi = \psi, \quad A_z = 0 \quad (\text{A19})$$

So another physical interpretation of the modified flux function is,

$$\mathbf{A} = \frac{\psi}{\rho} \hat{\varphi} \quad (\text{upto gauge}) \quad (\text{A20})$$

## Appendix B: Proof of Theorems

### 1. Dimensionless Reduction of The Problem

We make the system easier to analyze by making the following parameters dimensionless.

$$\begin{aligned} \tilde{x} &\equiv \frac{x}{r_s}, \quad \tilde{y} \equiv \frac{y}{r_s}, \quad \tilde{z} \equiv \frac{z}{z_s}, \quad \tilde{\psi} \equiv \frac{2\psi}{B_0 r_s^2}, \quad \tilde{\mathbf{B}} \equiv \frac{\mathbf{B}}{B_0}, \\ \tilde{\alpha} &\equiv \alpha k r_s, \quad m \equiv \frac{z_s^2}{r_s^2}, \quad \tilde{\alpha}_c \equiv \alpha_c k r_s = \frac{1}{\sqrt{m(1+2m)}} \end{aligned} \quad (\text{B1})$$

We will also denote normalized cartesian position vector to be,

$$\tilde{\mathbf{r}} \equiv (\tilde{x}, \tilde{y}, \tilde{z}) \quad (\text{B2})$$

In terms of these parameters,

$$\tilde{\mathbf{B}} = \left( \frac{\tilde{x}\tilde{z}}{\sqrt{m}}, \frac{(\tilde{y} - \tilde{\alpha}m)\tilde{z}}{\sqrt{m}}, 1 - 2(\tilde{x}^2 + \tilde{y}^2) - \tilde{z}^2 - \tilde{\alpha}\tilde{y} \right) \quad (\text{B3})$$

$$\tilde{\psi} = \mathbf{u}^2 (J - \mathbf{v}^2) \quad (\text{B4})$$

The following parameters remain the same so that we will use the same symbols for our analysis.

$$J = 1 - \tilde{\alpha}^2 (m+1)(2m-1)/9 \quad (\text{B5})$$

$$\mathbf{u} = (\tilde{x}, \tilde{y} - \tilde{\alpha}m, 0) \quad (\text{B6})$$

$$\mathbf{v} = \left( \tilde{x}, \tilde{y} + \frac{\tilde{\alpha}(1+m)}{3}, \tilde{z} \right) \quad (\text{B7})$$

$$\varphi = \tan^{-1} \left( \frac{\tilde{x}}{\tilde{y} - \tilde{\alpha}m} \right) \quad (\text{B8})$$

We will analyze everything for  $\tilde{\alpha} < \tilde{\alpha}_c$  before the phase transition so that it will be an implicit assumption.

### 2. Poincare-Hopf Theorem

For a compact and differentiable manifold  $M$  (such as flux surfaces) with a continuous vector field  $\mathbf{A}(\mathbf{r})$  on it, the indices of critical points  $\mathbf{r}_i$  (where  $\mathbf{A}(\mathbf{r}_i) = \mathbf{0}$ ) adds up to the Euler characteristics  $\chi(M)$  of the manifold.

$$\chi(M) = \sum_i \text{index}_{\mathbf{r}_i}(\mathbf{A}) \quad (\text{B9})$$

Here, the index of the critical point means how field lines behave near it. If they are elliptically orbiting 'O' points, it has an index of 1; if they are hyperbolic 'X' points, they have an index of -1, and so on. Spheres have  $\chi(M) = 2$ , torus have  $\chi(M) = 0$ , and discs have  $\chi(M) = 1$ . We have  $\psi$  surfaces or the area inside vector field  $\mathbf{B}$  as our compact differentiable manifolds for our work. We also have vector field  $\mathbf{B}$  available continuously embedded in these manifolds. So, the Poincare-Hopf theorem is applicable.

### 3. Lemmas

**Lemma 0** For every point in a connected field line,  $(\tilde{\psi}, \varphi)$  is same.

**Proof** It was already shown in [24]. Another way to reproduce the work is to calculate  $\nabla \tilde{\psi} \times \nabla \varphi$ . After long but straightforward calculations, it comes out as equal to  $\tilde{\mathbf{B}}$ . Now,  $\tilde{\mathbf{B}} = \nabla \tilde{\psi} \times \nabla \varphi \implies \tilde{\mathbf{B}} \cdot \nabla \tilde{\psi} = 0$  and  $\tilde{\mathbf{B}} \cdot \nabla \varphi = 0$ . This means if we follow a path always tangent to  $\tilde{\mathbf{B}}$ , or equivalently stay in a connected field line,  $\tilde{\psi}$  and  $\varphi$  will be conserved.  $\square$

**Lemma 1**  $\tilde{\psi}(\tilde{\mathbf{r}}) > 0 \iff \tilde{\mathbf{r}} \in E \setminus L$ ,  $\tilde{\psi}(\tilde{\mathbf{r}}) < 0 \iff \tilde{\mathbf{r}} \in E' \setminus L$  and  $\tilde{\psi}(\tilde{\mathbf{r}}) = 0 \iff \tilde{\mathbf{r}} \in \tilde{S}_1 \cup L$ . Where we defined inside, outside, and the surface of the sphere as,

$$E = \{\tilde{\mathbf{r}} : J > \mathbf{v}(\tilde{\mathbf{r}})^2\} \quad (\text{B10})$$

$$E' = \{\tilde{\mathbf{r}} : J < \mathbf{v}(\tilde{\mathbf{r}})^2\} \quad (\text{B11})$$

$$\tilde{S}_1 = \{\tilde{\mathbf{r}} : J = \mathbf{v}(\tilde{\mathbf{r}})^2\} \quad (\text{B12})$$

We defined the line

$$L = (0, \tilde{\alpha}m, \tilde{z}) \quad (\text{B13})$$

**Proof** If  $\tilde{\mathbf{r}} \in E \setminus L$  then  $\tilde{x}^2 + (\tilde{y} - \tilde{\alpha}m)^2 > 0$  and  $J - \mathbf{v}(\tilde{\mathbf{r}})^2 > 0$  which implies  $\tilde{\psi} > 0$ . If  $\tilde{\psi} > 0$  then either  $\tilde{x}^2 + (\tilde{y} - \tilde{\alpha}m)^2 < 0$  and  $J - \mathbf{v}(\tilde{\mathbf{r}})^2 < 0$  or  $\tilde{x}^2 + (\tilde{y} - \tilde{\alpha}m)^2 > 0$  and  $J - \mathbf{v}(\tilde{\mathbf{r}})^2 > 0$ . The first is not possible, and the former implies  $\tilde{\mathbf{r}} \in E$  and  $\tilde{\mathbf{r}} \notin L$ . This proves the first part of the lemma.

If  $\tilde{\mathbf{r}} \in E' \setminus L$  then  $\tilde{x}^2 + (\tilde{y} - \tilde{\alpha}m)^2 > 0$  and  $J - \mathbf{v}(\tilde{\mathbf{r}})^2 < 0$  which implies  $\tilde{\psi} < 0$ . If  $\tilde{\psi} < 0$  then either  $\tilde{x}^2 + (\tilde{y} - \tilde{\alpha}m)^2 < 0$  and  $J - \mathbf{v}(\tilde{\mathbf{r}})^2 > 0$  or  $\tilde{x}^2 + (\tilde{y} - \tilde{\alpha}m)^2 > 0$  and  $J - \mathbf{v}(\tilde{\mathbf{r}})^2 < 0$ . The first is not possible, and the former implies  $\tilde{\mathbf{r}} \in E'$  and  $\tilde{\mathbf{r}} \notin L$ . This proves the second part of the lemma.

If  $\tilde{\mathbf{r}} \in E \cup L$  then  $\tilde{x}^2 + (\tilde{y} - \tilde{\alpha}m)^2 = 0$  or  $J - \mathbf{v}(\tilde{\mathbf{r}})^2 = 0$  both of which imply  $\tilde{\psi} = 0$ . If  $\tilde{\psi} = 0$  then either  $\tilde{x}^2 + (\tilde{y} - \tilde{\alpha}m)^2 = 0$  or  $J - \mathbf{v}(\tilde{\mathbf{r}})^2 = 0$  This implies  $\tilde{\mathbf{r}} \in E \cup L$ . This proves the third part of the lemma.  $\square$

**Lemma 2** Critical points, defined by  $\mathbf{r}$  such that  $\tilde{\mathbf{B}}(\tilde{\mathbf{r}}) = 0$ , are either the circle  $C_{crit}$  or  $P_{crit}$  isolated points that fulfill,

$$C_{crit} \subset E, P_{crit} \subset \tilde{S}_{out} \cap L \quad (\text{B14})$$

Where,

$$C_{crit} \equiv \{\tilde{\mathbf{r}} : 1 - 2(\tilde{x}^2 + \tilde{y}^2) - \alpha\tilde{y} = 0, \tilde{z} = 0\} \quad (\text{B15})$$

$$P_{crit} = \left\{ (0, \tilde{\alpha}m, s\sqrt{1 - \frac{\tilde{\alpha}^2}{\tilde{\alpha}_c^2}}) \mid s \in \{+1, -1\} \right\} \quad (\text{B16})$$

**Proof** Critical points must fulfill  $\tilde{\mathbf{B}}(\tilde{\mathbf{r}}) = 0$  condition.

$$\begin{aligned} \frac{\tilde{x}\tilde{z}}{\sqrt{m}} = 0, \quad \frac{\tilde{y} - \tilde{\alpha}m}{\sqrt{m}}\tilde{z} = 0, \\ 1 - 2(\tilde{x}^2 + \tilde{y}^2) - \tilde{z}^2 - \tilde{\alpha}\tilde{y} = 0 \end{aligned} \quad (\text{B17})$$

For case  $\tilde{z} = 0$ , we can show that critical points form the following circle in the  $\tilde{z} = 0$  plane after some calculations.

$$\tilde{x}^2 + \left(\tilde{y} + \frac{\tilde{\alpha}}{4}\right)^2 = R_1^2, \text{ where, } R_1 = \sqrt{\frac{1}{2} + \frac{\tilde{\alpha}^2}{16}} \quad (\text{B18})$$

The intersection of  $\tilde{S}_1$  sphere and  $\tilde{z} = 0$  plane is also a circle.

$$\tilde{x}^2 + \left(\tilde{y} + \frac{\tilde{\alpha}(1+m)}{3}\right)^2 = R_2^2 \quad (\text{B19})$$

$$R_2 \equiv \sqrt{1 - \frac{\tilde{\alpha}^2}{9}(m+1)(2m-1)} \quad (\text{B20})$$

The distance between the center of the circles can be shown to be

$$d = \frac{\tilde{\alpha}(1+4m)}{12} < \frac{\tilde{\alpha}_c(1+4m)}{12} \quad (\text{B21})$$

Radius of the circle in Eq. (B18)

$$R_1 < \sqrt{\frac{1}{2} + \frac{\tilde{\alpha}_c^2}{16}} = \frac{(1+4m)\tilde{\alpha}_c}{4} \quad (\text{B22})$$

$$\implies R_1 + d < \frac{1+4m}{3\tilde{\alpha}_c} \quad (\text{B23})$$

And of circle in Eq. (B20),

$$R_2 > \sqrt{1 - \frac{\tilde{\alpha}_c^2}{9}(m+1)(2m-1)} = \frac{1+4m}{3\tilde{\alpha}_c} \quad (\text{B24})$$

$$\implies R_2 > R_1 + d \quad (\text{B25})$$

This means the circle from Eq. (B18) is fully inside the circle Eq. (B20). So all  $\tilde{\mathbf{B}}(\tilde{\mathbf{r}}) = 0$  points satisfy  $\tilde{\mathbf{r}} \in E$  for  $\tilde{\alpha} < \tilde{\alpha}_c$ . Thus  $C_{crit} \subset E$

Case  $\tilde{z} \neq 0$ ,  $\implies \tilde{x} = 0, \tilde{y} = \tilde{\alpha}m \implies \tilde{\mathbf{r}} \in L$ , and  $1 - 2(\tilde{\alpha}m)^2 - \tilde{\alpha}^2m = 0$ . This implies  $\tilde{z} = \sqrt{1 - \alpha^2/\alpha_c^2}$ . After some calculations,

$$\begin{aligned} \mathbf{v} &= (\tilde{\alpha}m + \tilde{\alpha}(1+m)/3)^2 + 1 - m(1+2m)\tilde{\alpha}^2 \\ &= 1 - \frac{\alpha^2}{9}(m+1)(2m-1) = J \end{aligned} \quad (\text{B26})$$

Thus,  $\tilde{\mathbf{r}} \in \tilde{S}_{out} \implies P_{crit} \subset \tilde{S}_{out} \cap L$ .  $\square$

**Lemma 3** All field lines with same  $(\tilde{\psi}, \varphi)$  are connected lines and all flux surfaces with same  $\tilde{\psi}$  are connected surfaces.

**Proof** We first show that all points in a field line  $(\tilde{\psi}, \varphi)$  are connected. we define the cylindrical co-ordinate  $(u, \varphi, \tilde{z})$  such that  $\tilde{x} = \tilde{u} \sin \varphi$ ,  $\tilde{y} = \tilde{u} \cos \varphi + \tilde{\alpha}m$ ,  $\tilde{z} = \tilde{z}$ . Here  $u > 0$  and  $\varphi \in [0, 2\pi)$  In terms of these co-ordinates,

$$\tilde{\psi} = u^2(I - u^2 - a u \cos \varphi - \tilde{z}^2), \quad (\text{B27})$$

$$\text{where, } I = 1 - \tilde{\alpha}^2/\tilde{\alpha}_c^2 > 0,$$

$$\text{and, } a \equiv 2\tilde{\alpha}(1+4m)/3 > 0$$

We first focus on  $\tilde{z} > 0$  on a single field line  $(\tilde{\psi}, \varphi)$ . The  $(\tilde{\psi}, \varphi)$  pair is a constant for a field line. This implies,

$$\tilde{z}^2 = I - u^2 - a u \cos \varphi - \frac{\tilde{\psi}}{u^2} \quad (\text{B28})$$

$$\implies \tilde{z} \frac{d\tilde{z}}{du} = -2u - a \cos \varphi + \frac{2\tilde{\psi}}{u^3} \quad (\text{B29})$$

We know  $u > 0$  because  $\tilde{\psi} \neq 0$  implies the point is not on  $L$  line, hence  $u \neq 0$ . Furthermore,  $z > 0$  as per assumption. So, the derivative exists for all points in the domain. Now, we prove that the domain of  $\tilde{z}(u)$  is connected. We first study the points where  $z(u) = 0$ . This condition is satisfied when,

$$\tilde{\psi} = \Psi(u), \quad \Psi(u) \equiv u^2(I - u^2 - a u \cos \varphi) \quad (\text{B30})$$

Have real solutions that happen when  $\tilde{\psi}$  intersects  $\Psi(u)$ . We now set the derivative  $d\Psi(u)/du$  to 0 to find the critical points.

$$u_0 = 0 \quad u_{\pm} = \frac{1}{8} \left( -3a \cos \varphi \pm \sqrt{9a^2 \cos^2 \varphi + 32I} \right) \quad (\text{B31})$$

Given that  $A > 0$  and  $I > 0$ , we have  $9A^2 \cos^2 \varphi + 32 > (3A|\cos \varphi|)^2$ . This gives us,

$$u_+ > \frac{3a}{8} (|\cos \varphi| - \cos \varphi) > 0 \quad (\text{B32})$$

$$\text{and, } u_- < -3a(|\cos \varphi| + \cos \varphi) < 0 \quad (\text{B33})$$

So, only one solution fulfills the  $u > 0$  condition. So, only a single critical point exists. It is not essential for our analysis if  $u_c$  is a minima or a maxima; the conclusions remain the same. Given that only a single critical point exists,  $\tilde{\psi}$  intersects the  $\Psi(u)$  vs  $u$  plot in 0, 1 or 2 points. Furthermore,  $u$  can not have an unbounded domain as that makes  $\tilde{z}(u)^2 < 0$  for large enough  $u$ .

1. 0 points. For this case, the domain of  $u$  is  $(0, \infty)$ , which is unbounded and hence impossible.
2. 1 Point, let us denote the point  $u_0$ . The domain thus can be  $(0, u_0)$  or  $(u_0, \infty)$ .  $(u_0, \infty)$  is impossible because it is not bounded. So it must be  $(0, u_0)$  which is simply connected.
3. 2 points, let us denote the points  $u_1$  and  $u_2$  such  $u_2 > u_1$ . Now, the domains can be  $(u_1, u_2)$  or  $(0, u_1) \cup (u_2, \infty)$ .  $(0, u_1) \cup (u_2, \infty)$  is impossible because it is not bounded. So it must be  $(u_1, u_2)$  which is simply connected.

While ruling out 0 points, we have also proven a strong claim: a field line must have at least 1 point where  $z = 0$ .

Now,  $\tilde{z}(u)$  is a continuous function of  $u$  with a simply connected domain. So, the portion of the field line with  $z > 0$  is connected. Now, the system is mirror symmetric with respect to the  $z = 0$  plane. So  $z > 0$  and  $z < 0$  portion of the field line  $(\tilde{\psi}, \varphi)$  intersect  $z = 0$  points in the same points. Thereby, all points in any field line are connected. This proves first part of the lemma.

Now, we show that all field lines have a continuous path connecting them. We define the following path in  $x > 0$  part of the space.

$$P_+(\varphi) = (u_0, \varphi, \tilde{z}_0(\varphi)), \quad \text{for all } \varphi \in [0, \pi) \quad (\text{B34})$$

$$\text{where, } \tilde{z}_0(\varphi) = \sqrt{I - u_0^2 - au_0 \sin \varphi - \frac{\tilde{\psi}}{u_0^2}}$$

It is clear that path  $P(\varphi)$  exists entirely on  $\psi$  surface because after some calculations one can show that,

$$\tilde{\psi} = u_0^2(I - u_0^2 - au_0 \cos \varphi - \tilde{z}_0(\varphi)^2) \quad (\text{B35})$$

We define  $u_0$  as the  $u$  component of a point on the field line with the lowest possible value of  $\varphi$ , which we denote as  $\varphi_0$ . Additionally, we require that the point satisfies

$$z_0(\varphi_0) = 0 \quad (\text{B36})$$

We have already shown that such a point must exist while ruling out the possibility of zero intersection points of a field line on the  $z = 0$  plane. The proof of the claim presupposed that the point exists on a field line. The point may not exist on any field line, but in that case, the vector field in its neighborhood must tend to 0. It thus must be a critical point, which is also guaranteed to have  $z_0(\varphi) = 0$ . We know,  $\cos \varphi$  is a strictly decreasing function of  $\varphi$  in  $[0, \pi)$  domain. So, for any field line  $\varphi \geq \varphi_0$ ,

$$\cos \varphi \leq \cos \varphi_0 \implies z_0(\varphi)^2 \geq z_0(\varphi_0)^2 = 0 \quad (\text{B37})$$

This means  $z_0(\varphi)$  is continuous and real in  $\varphi \in [-\pi/2, \varphi_0]$  range. So, the path  $P_+(\varphi)$  is a continuous path on  $\psi$  surface that connects  $(u_0, \varphi_0, z_0(\varphi_0))$  point in  $\varphi_0$  plane to  $(u_0, \varphi, z_0(\varphi))$  point in  $\varphi$  plane.

We choose a point  $c = (u_0, \varphi_1, z_0(\varphi_1))$  on the  $\varphi = \varphi_1 < \varphi_0$  plane. Any point on  $P_+(\varphi)$  line is on the  $\tilde{\psi}$  which includes  $c$ . Field lines are intersections of  $\tilde{\psi}$  and  $\varphi$  planes. So, this point is on the field line  $(\tilde{\psi}, \varphi_1)$ .

Hence there is a continuous connected path  $P_+(\varphi)$  on  $\psi$  surface connecting all field lines within range  $[0, \varphi_0]$  on the  $\psi$  surface. Because of the mirror symmetry of the system on the  $\tilde{x} = 0$  plane, the mirror version of the path  $P_-$  will connect all points on the  $\tilde{x} < 0$  side. Because of mirror symmetry,  $P_{\pm}$  must intersect  $x = 0$  on the same points, thereby connecting one to the other. We define the connected and continuous path created from gluing  $P_{\pm}$  with each other as  $P$ . So, a continuous path connects all field lines on a single  $\tilde{\psi}$  surface.

We choose any two points  $p_1, p_2 \in \tilde{\psi}$  surface such that  $p_1 \in (\tilde{\psi}, \varphi_1)$  and  $p_2 \in (\tilde{\psi}, \varphi_2)$  field lines. Given that all points on a field line are connected, we can find a continuous path  $L_1$  to reach the point  $q_1$  on  $(\tilde{\psi}, \varphi_1)$  that intersects with the continuous  $P$  path that connects all field lines.  $q_1$ 's existence is ensured by all field lines being connected to  $P$ . Then, we can use the connected  $P$  path to reach  $(\tilde{\psi}, \varphi_2)$  field line as  $P$  connects all field lines. Let's denote the point  $P$  intersects on  $(\tilde{\psi}, \varphi_2)$  as  $q_2$ . Given that all points in a field line are connected, we can reach  $p_2$  from  $q_2$  via a continuous path  $L_2$ . So, a continuous path  $L_1 - P - L_2$  connects  $p_1$  and  $p_2$ . So any two points on  $\tilde{\psi}$  surfaces are connected via a connected path on  $\tilde{\psi}$  surface. So, all flux surfaces  $\tilde{\psi} \neq 0$  are connected surfaces.

The  $\tilde{\psi} \neq 0$  surface is  $\tilde{S}_1 \cup L$ .  $\tilde{S}_1$  is a sphere and hence connected, and  $L$  is a line which is also connected. We observe  $u = 0$  on  $L$ . So, using the line  $L$  intersects  $\tilde{S}_1$  on

$$\tilde{z} = \pm \sqrt{I - u^2 - au \cos \varphi} = \pm \sqrt{1 - \frac{\tilde{a}^2}{\tilde{a}_c^2}} \quad (\text{B38})$$

which exists for  $\tilde{\alpha} < \tilde{\alpha}_c$  so the flux surface remains connected.  $\square$

**Lemma 4** All field lines and flux surfaces with  $\tilde{\psi} < 0$  are open.

**Proof** Let us focus on the field line  $(\tilde{\psi}, \varphi)$  in  $\varphi$  plane such that  $\tilde{\psi} < 0$ . We again use the cylindrical coordinate  $(u, \varphi)$  used in *lemma 3*. In terms of that, coordinate  $\tilde{z}^2$  is given by Eq. (B28). For  $\tilde{\psi} < 0$ , the  $-\tilde{\psi}/u^2$  term  $\rightarrow \infty$  as  $u \rightarrow 0$  which gives us  $\tilde{z} \rightarrow \pm\infty$ . This means the field line is not bounded. Given that the field line is connected because of *lemma 3*, the field line is thus open. Given that all field lines on the flux surface are open, the flux surface is thus open.  $\square$

**Lemma 5** Any flux surfaces with  $\tilde{\psi} > 0$  are closed and can be covered by a finite volume and hence compact.

**Proof** From *lemma 1*, all points with  $0 < \tilde{\psi}$  exist inside the spherical finite region. So, any surface they create also exists in the closed finite region. Thus, all flux surfaces with  $0 < \tilde{\psi}$  are closed and can be covered by a volume.  $\square$

**Lemma 6** Flux surfaces with  $0 < \tilde{\psi} < \tilde{\psi}_-$  are topologically torus. Here,

$$\tilde{\psi}_- = \tilde{\psi}(0, \tilde{y}_+, 0) \text{ and, } \tilde{y}_+ = \frac{-\tilde{\alpha} + \sqrt{\tilde{\alpha}^2 + 8}}{4} \quad (\text{B39})$$

**Proof** The only critical points are  $C_{crit} \subset E$  or  $P_{crit} \subset \tilde{S}_{out}$ . But any point on  $\tilde{S}_{out}$  have  $\tilde{\psi} = 0$  and thus won't intersect with  $\tilde{\psi} > 0$  surfaces. So we will only have to consider  $C_{crit}$  circle. So, we may simplify the set of equations by

$$\tilde{\psi} = (\tilde{x}^2 + (\tilde{y} - \tilde{\alpha}m)^2) \left( J - \tilde{x}^2 - \left( \tilde{y} + \frac{\tilde{\alpha}(m+1)}{3} \right)^2 \right) \quad (\text{B40})$$

$$1 - 2(\tilde{x}^2 + \tilde{y}^2) - \tilde{\alpha}\tilde{y} = 0 \quad (\text{B41})$$

$\tilde{x}^2 \geq 0$  and the second equation puts a restriction on  $\tilde{y}$  by

$$1 - 2\tilde{y}^2 - \tilde{\alpha}\tilde{y} \geq 0 \quad (\text{B42})$$

$$\implies \tilde{y}_- \leq \tilde{y} \leq \tilde{y}_+ \text{ where, } \tilde{y}_{\pm} \equiv \frac{-\tilde{\alpha} \pm \sqrt{\tilde{\alpha}^2 + 8}}{4} \quad (\text{B43})$$

Now replacing  $\tilde{x}^2$  gives us after some simplifying steps,

$$\tilde{\psi} = 12(1 + 2\tilde{\alpha}^2m^2 - \tilde{\alpha}\tilde{y}(1 + 4m)) \times (3 - 2\tilde{\alpha}^2m(m+1) - \tilde{\alpha}\tilde{y}(1 + 4m)) \quad (\text{B44})$$

Solving for  $\tilde{y}$  gives us,

$$\tilde{y} = \tilde{h}_{\pm} \equiv \frac{2 - \tilde{\alpha}^2m \pm \sqrt{(m(2m+1)\tilde{\alpha}^2 - 1)^2 + \tilde{\psi}/12}}{\tilde{\alpha}(1 + 4m)} \quad (\text{B45})$$

We now focus on the first possible solution  $\tilde{y} = \tilde{h}_+$ . After some long calculations, for  $\tilde{\psi} > 0$  and  $\tilde{\alpha} < \tilde{\alpha}_c = 1/\sqrt{m(1+2m)}$  we have,

$$\begin{aligned} \tilde{h}_+ &> \frac{2 - \tilde{\alpha}^2m \pm \sqrt{(m(2m+1)\tilde{\alpha}^2 - 1)^2 + \tilde{\psi}/12}}{\tilde{\alpha}(1 + 4m)} \\ &= \frac{3 - 2\tilde{\alpha}^2m(1+m)}{(1+4m)\tilde{\alpha}} \equiv q(\tilde{\alpha}) \end{aligned} \quad (\text{B46})$$

$q(\tilde{\alpha})$  is a strictly decreasing function of  $\tilde{\alpha}$  for  $\tilde{\alpha} > 0$ . Furthermore,

$$\frac{d\tilde{y}_+}{d\tilde{\alpha}} = -\frac{1}{4} \left( 1 + \frac{\tilde{\alpha}}{\sqrt{\tilde{\alpha}^2 + 8}} \right) \quad (\text{B47})$$

So,  $\tilde{y}_+$  is a strictly decreasing function of  $\tilde{\alpha}$  for  $\tilde{\alpha} > 0$ . So, they intersect only once. Before that intersection, the initially larger function remains larger, and after that intersection, it becomes permanently smaller. At  $\tilde{\alpha} = 0$ ,  $q(\tilde{\alpha}) \rightarrow \infty$  and  $\tilde{y}_+ = 1/\sqrt{2}$ . So until the intersection point  $q(\tilde{\alpha}) > \tilde{y}_+(\tilde{\alpha})$ . After long but straightforward calculations, we can show that

$$q(\tilde{\alpha}_c) = \tilde{y}_+(\tilde{\alpha}_c) = \sqrt{\frac{m}{1+2m}} \quad (\text{B48})$$

So for  $0 < \tilde{\alpha} < \tilde{\alpha}_c$ ,

$$\tilde{y}_+ < q(\tilde{\alpha}) < \tilde{h}_+ = \tilde{y} \quad (\text{B49})$$

$$(\text{B50})$$

So, the inequality in Eq. (B43) is violated. Thus, there are no intersections between  $\tilde{y} = \tilde{h}_+$  and the critical point circles, and we don't have to worry about it. We focus on the other solution  $\tilde{y} = \tilde{h}_-$  now. For  $\tilde{\psi} > 0$ ,  $\tilde{h}_-$  is well defined and strictly decreasing with  $\tilde{\psi}$ . The condition for which the intersection happens will require  $\tilde{h}_-$  to fulfill,

$$\tilde{y}_- < \tilde{h}_- < \tilde{y}_+ \quad (\text{B51})$$

$$\implies \tilde{\psi}(0, \tilde{y}_-, 0) > \tilde{\psi}(0, \tilde{h}_-, 0) > \tilde{\psi}(0, \tilde{y}_+, 0) \quad (\text{B52})$$

After some calculations, it can be shown that,

$$\tilde{\psi}(0, \tilde{h}_-, 0) = \tilde{\psi} \quad (\text{B53})$$

$$\implies \tilde{\psi}_- < \tilde{\psi} < \tilde{\psi}_+ \quad (\text{B54})$$

Here, we have defined,

$$\tilde{\psi}_{\pm} \equiv \tilde{\psi}(0, \tilde{y}_{\mp}, 0) \quad (\text{B55})$$

We already know that  $(0, \tilde{y}_{\pm}, 0)$  is a critical point and by *lemma 2* we have  $(0, \tilde{y}_{\pm}, 0) \in \tilde{E}$  and  $\notin \tilde{L}$ . So,  $(0, \tilde{y}_{\pm}, 0) \in \tilde{E} \setminus \tilde{L}$  which by *lemma 1* gives us  $0 < \tilde{\psi}_{\pm}$  and specifically  $0 < \tilde{\psi}_-$ . So, the inequality  $0 < \tilde{\psi} < \tilde{\psi}_-$  is well defined.

Flux surfaces in the range  $0 < \tilde{\psi} < \tilde{\psi}_-$  are compact, yet they have no critical point on them. So, according to the Poincare-Hopf theorem, the total index must add up to  $\chi(M) = 0$ . A torus is the only connected surface in

$\mathbb{R}^3$  with  $\chi(M) = 0$ . Our surfaces are connected because of *lemma 3*.  $\square$

**Lemma 7** Flux surfaces with  $\tilde{\psi}_- < \tilde{\psi} < \tilde{\psi}_+$  are topologically simply connected or spherical.

**Proof** From Eq. (B54), we know that, for  $\tilde{\psi}_- < \tilde{\psi} < \tilde{\psi}_+$  the flux surface intersects with exactly two critical points  $(\pm(1 - \tilde{\alpha}\tilde{h}_-(\tilde{\psi}))/2 - \tilde{h}_-(\tilde{\psi})^2, \tilde{h}_-(\tilde{\psi}), 0)$  with the circle  $C_{crit}$ . As before, given  $\tilde{\psi} > 0$ , there is no intersection with  $P_{crit}$ . Thus only two critical points exist on these surfaces. Because  $\tilde{\psi}$  has a symmetry across the  $\tilde{x}$  axis, the critical points are identical, and we can focus on a single one.

The field lines around these critical points lie on the flux surface by theorem 2 and can thus be used to study the index of the critical points. The field line is given by the equation,

$$\frac{d\tilde{\mathbf{r}}}{ds} = \tilde{\mathbf{B}}(\tilde{\mathbf{r}}) \quad (\text{B56})$$

We do a first order expansion  $|\delta\tilde{\mathbf{r}}| \ll |\tilde{\mathbf{r}}|$  in the neighborhood of the critical points  $\tilde{\mathbf{r}}$ . Linearizing the equations and using the critical condition  $\tilde{\mathbf{B}}(\tilde{\mathbf{r}}) = 0$  required gives us,

$$\frac{d}{ds}(\delta\tilde{\mathbf{r}}) = \mathbf{M} \delta\tilde{\mathbf{r}}, \quad (\text{B57})$$

$$\mathbf{M} \equiv \begin{pmatrix} 0 & 0 & \tilde{x}/\sqrt{m} \\ 0 & 0 & (\tilde{y} - \tilde{\alpha}m)/\sqrt{m} \\ -4\tilde{x} & -4\tilde{y} - \tilde{\alpha} & 0 \end{pmatrix}$$

For eigenvalue  $\omega$ , replacing  $\tilde{x}^2$  with  $1/2 - \tilde{\alpha}\tilde{y}/2 - \tilde{y}^2$  we get the secular equation,

$$\omega \left( \omega^2 + \frac{f(\tilde{\alpha}, \tilde{y})}{\sqrt{m}} \right) = 0, \quad (\text{B58})$$

$$\text{where, } f(\tilde{\alpha}, \tilde{y}) \equiv 2 - (1 + 4m)\tilde{\alpha}\tilde{y} - \tilde{\alpha}^2m$$

Now,  $\omega = 0$  gives us a stationary point and is irrelevant to our discussion. If the orbit is an ellipse, then  $\omega$  must be imaginary; thus,  $\omega^2 < 0$ . This is true only if and only if the function,

$$f(\tilde{\alpha}, \tilde{y}) > 0 \quad (\text{B59})$$

The function  $f(\tilde{\alpha}, \tilde{y}) > 0$  needs to be fulfilled only within the following region

$$\{(\tilde{\alpha}, \tilde{y}) : \tilde{y}_-(\tilde{\alpha}) < \tilde{y} < \tilde{y}_+(\tilde{\alpha}), \tilde{\alpha} < \tilde{\alpha}_c\} \quad (\text{B60})$$

because  $\tilde{y}$  belongs to the critical points and is therefore defined only within this range. As for the second inequality, it is there to enforce  $\tilde{\alpha} < \tilde{\alpha}_c$ .  $f(\tilde{\alpha}, \tilde{y})$  is a strictly decreasing function of  $\tilde{y}$ . So  $\tilde{y} < \tilde{y}_+(\tilde{\alpha})$  dictates,

$$f(\tilde{\alpha}, \tilde{y}) > f(\tilde{\alpha}, \tilde{y}_+(\tilde{\alpha})) \equiv g(\tilde{\alpha}) \quad (\text{B61})$$

After some calculation, we can show the following,

$$\frac{dg}{d\tilde{\alpha}} = \frac{\tilde{\alpha}}{4} \left( 1 - (1 + 4m) \left( \frac{\sqrt{\tilde{\alpha}^2 + 8}}{\tilde{\alpha}} + \frac{\tilde{\alpha}}{\sqrt{\tilde{\alpha}^2 + 8}} \right) \right) \quad (\text{B62})$$

From the inequality of arithmetic mean vs geometric mean, we know,

$$\frac{\sqrt{\tilde{\alpha}^2 + 8}}{\tilde{\alpha}} + \frac{\tilde{\alpha}}{\sqrt{\tilde{\alpha}^2 + 8}} \geq 2 \quad (\text{B63})$$

$$\implies \frac{dg}{d\tilde{\alpha}} \leq -\frac{\tilde{\alpha}(1 + 8m)}{4} \quad (\text{B64})$$

So for  $\tilde{\alpha} > 0$ ,  $g(\tilde{\alpha})$  is a strictly decreasing function of  $\tilde{\alpha}$ . So,

$$\tilde{\alpha} < \tilde{\alpha}_c \implies g(\tilde{\alpha}) > g(\tilde{\alpha}_c) \quad (\text{B65})$$

After some calculations, we can show that  $g(\tilde{\alpha}_c) = 0$ , hence  $g(\tilde{\alpha}) > 0$ . This proves,

$$f(\tilde{\alpha}, \tilde{y}) > g(\tilde{\alpha}) > 0 \quad (\text{B66})$$

So, the eigenvalues are imaginary; thus, the orbits around the critical points are elliptical. This means both of the critical points have index 1. From *lemma 4*, we know that any surfaces with  $\tilde{\psi} > 0$  are compact. Thus, the Euler characteristic of the manifold is  $\chi(M) = 1 + 1 = 2$  [25, 26]. All flux surfaces are connected because of *lemma 3*. Only possible connected surfaces in  $\mathbb{R}^3$  with  $\chi(M) = 2$  have spherical topology. So all  $\tilde{\psi}_- < \tilde{\psi} < \tilde{\psi}_+$  surfaces are topologically simply connected or spherical.  $\square$

**Lemma 8**  $\psi_+$  is the maximum of  $\psi$  and flux surfaces do not exist beyond this. Here,

$$\tilde{\psi}_+ = \tilde{\psi}(0, \tilde{y}_-, 0) \quad \text{and, } \tilde{y}_- = \frac{-\tilde{\alpha} - \sqrt{\tilde{\alpha}^2 + 8}}{4} \quad (\text{B67})$$

**Proof** We again work in polar co-ordinate  $(u, \varphi)$ . In Eq. (B3),  $\tilde{\psi}$  is a strictly decreasing function of  $\tilde{z}^2$  and  $\cos \varphi$ . So setting  $\tilde{z} = 0$  and  $\cos \varphi = -1$  maximizes the function. In Eq. (B31), we already calculated the value of  $u = u_+ > 0$  for which  $d\tilde{\psi}/du = 0$  in Eq. (B31) in any  $\varphi$  plane. We set  $\sin \varphi = -1$  plane, and after some calculations, we get,

$$u = \frac{(1 + 4m)\tilde{\alpha} \pm \sqrt{\tilde{\alpha}^2 + 8}}{4} \quad (\text{B68})$$

For  $\tilde{\alpha} < \tilde{\alpha}_c$ ,

$$\tilde{\alpha}^2 < \tilde{\alpha}_c^2 = \frac{1}{m(1 + 2m)} = \frac{8}{(1 + 4m)^2 - 1} \quad (\text{B69})$$

$$\implies (1 + 4m)\tilde{\alpha} - \sqrt{8 + \tilde{\alpha}^2} < 0 \quad (\text{B70})$$

So,  $u = ((1 + 4m)\tilde{\alpha} - \sqrt{\tilde{\alpha}^2 + 8})/4$  is a negative solution and hence not possible as  $u > 0$ . The other two solutions gives us  $\tilde{y} = am$  or  $\tilde{y} = y_-$ . So the maximum occurs at  $(0, \tilde{\alpha}m, 0)$  or  $(0, \tilde{y}_\pm, 0)$ . The first possibility  $\tilde{\xi} = 0$  gives us  $\tilde{\psi} = 0$ . The other possibility gives us are  $\tilde{\psi}(0, \tilde{y}_-, 0) = \tilde{\psi}_+$ . We have already shown  $0 < \tilde{\psi}_- < \psi_+$ .

So  $\tilde{\psi}_+$  is the maximum possible value of  $\tilde{\psi}$ . So, no surfaces exist beyond  $\tilde{\psi}_+$ .  $\square$

**Lemma 9** Simply connected flux surfaces (and associated field lines) with  $\tilde{\psi} < \tilde{\psi}_-$  stay strictly in the interior of  $\tilde{\psi}_-$  surface.

**Proof**  $\tilde{\psi}_- > 0$ , so by *lemma 4*, it is a closed surface. Thus, the concept of exterior and interior of  $\tilde{\psi}_-$  is well defined, which proves the implicit claim that  $F, F', \partial F$  are disjoint sets. So, any flux surface must be either fully in the interior of  $\tilde{\psi}_-$ , fully outside of  $\tilde{\psi}_-$ , or it may have an intersection.

Any  $\tilde{\psi} > \tilde{\psi}_-$  surface cannot have any intersection with  $\tilde{\psi}_-$ , and the intersection points will coincide with intersection points with  $\tilde{\psi}_-$ , leading to  $\tilde{\psi} = \tilde{\psi}_- \not\neq \tilde{\psi}_-$ , which is a contradiction.

If  $\tilde{\psi}$  is fully in the exterior of  $\tilde{\psi}_-$ , then it fully contains  $\tilde{\psi}_-$ , which in turn includes the  $(0, \tilde{y}_+, 0)$  on  $\tilde{\psi}_+$ . Given that  $(0, \tilde{y}_+, 0)$  is inside a closed surface  $\tilde{\psi}$ , there are two points on  $\tilde{\psi}$  that intersect with the  $\tilde{y}$ -axis. While proving *lemma 8*, we have shown that there are two maxima on  $\tilde{y} = \tilde{y}_\pm$  and a minimum at  $\tilde{y} = 0$ . So, for  $\tilde{y} > \tilde{y}_+$ ,  $\tilde{\psi}$  decreases. Thus,  $\tilde{\psi} < \tilde{\psi}_-$ , which is not possible. So,  $\tilde{\psi}$  must be fully in the interior of  $\tilde{\psi}_-$ .  $\square$

**Lemma 10** Torus flux surfaces (and associated field lines) with  $0 < \tilde{\psi} < \tilde{\psi}_-$  stay strictly in the exterior of  $\tilde{\psi}(\tilde{\mathbf{r}}) = \tilde{\psi}_-$  and the interior of  $\tilde{S}_1$ .

**Proof** Simply connected flux surfaces with  $\tilde{\psi} > \tilde{\psi}_-$  are inside  $\tilde{\psi}(\tilde{\mathbf{r}}) = \tilde{\psi}_-$ , so torus flux surfaces must exist outside of that boundary. However, they are not open and cannot exist outside or on  $\tilde{\psi} = 0$ . Thus, they must exist in the interior of  $\tilde{S}_1$ .  $\square$

**Lemma 11** All field lines with  $\psi > 0$ , or equivalently  $\subset E \setminus L$ , are closed.

**Proof** All flux surfaces with  $\psi > 0$  are torus or spherical in topology. Field lines are the intersection of constant  $\varphi$  planes and flux surfaces, so they must intersect in closed loops, given that flux surfaces are torus or spheres in topology.  $\square$

#### 4. Finalizing the Proof

We have proved all the claims in developing the lemmas. All that remains is to collect them systemically. First, we convert  $\tilde{\psi}_\pm \rightarrow \psi_\pm$  and  $\tilde{y}_\pm \rightarrow y_\pm$  in dimensioned form which gives us Eq. (13). The dimensioned form for  $\tilde{S}_1$  becomes the outer separatrix  $S_{out}$ . The inner separatrix  $S_{in}$  has the equation  $\psi(\mathbf{r}) = \psi_-$ . We now prove the *theorems*.

1. Maximum value of  $\psi$  is  $\psi_+$  is because of *lemma 8* meaning the domain of  $(\psi, \varphi)$  is  $(-\infty, \psi_+) \times [0, 2\pi)$ . For a connected field line,  $(\psi, \varphi)$  is same everywhere because of *lemma 0*. And all points with same

$(\psi, \varphi)$  pair are part of the same connected field line because of *lemma 3*. Thus, in this domain, there is a one-to-one correspondence between  $(\psi, \varphi)$  pair and a single connected field line.  $\blacksquare$

2. For  $\psi \in (-\infty, 0)$ , the flux surfaces and field lines are outside of  $S_{out}$  because of *lemma 1* and open because of *lemma 4*.  $\blacksquare$
3. For  $\psi \in (0, \psi_-)$ , the flux surfaces are closed and topologically torus because of *lemma 6*. The flux surfaces and field lines are outside  $S_{in}$  but inside  $S_{out}$  because of *lemma 10*. Field lines are closed because of *lemma 11*.  $\blacksquare$
4. For  $\psi \in (\psi_-, \psi_+)$ , the flux surfaces are closed and topologically spherical because of *lemma 7*. The flux surfaces and field lines are inside  $S_{out}$  because of *lemma 9*. Field lines are closed because of *lemma 11*.  $\blacksquare$

#### Appendix C: Generality of the Perturbation Model

The perturbation in Eq. (3) represents a much broader class.

**Claim:** Any topological behavior of the vortex under slowly spatially varying, closure-preserving and zero vorticity perturbations is captured by Eq. (3).

Zero vorticity in magnetic systems means the absence of current along the field lines, so it can be interpreted as vacuum condition in context of magnetic field. Slowly spatially varying mean perturbations with small wavenumber  $k$  such that  $kr, kz$  are small in the region of interest, a reasonable assumption for weak perturbations. So, only terms of order  $\mathcal{O}(kr_s + kz_s)$  will be kept. Perturbations can be divided into odd- and even-parity types. Weak ( $\alpha < 0.05$ ) odd-parity perturbations were conjectured to preserve the closedness of field lines in the FRC-RMF system in [4]. [23] shows that even-parity perturbations open the field-line structure. Thus, the term ‘‘closure preserving’’ is *defined* to be equivalent to odd parity in this paper.

**Proof of Claim:** We write perturbation in cylindrical co-ordinate  $\delta\mathbf{B} \equiv (\delta B_r, \delta B_\phi, \delta B_z)$ . We defined the Fourier transformation of  $\delta\mathbf{B}$  in the  $(n, k)$  space to be,

$$\delta\hat{\mathbf{B}}(r, n, k) = \int \int \delta\mathbf{B}(r, \phi, z) e^{-in\phi - ikz} d\phi dz \quad (C1)$$

As we are requiring the perturbation to vary slowly spatially, this means we will need  $\delta\hat{\mathbf{B}}(r, n, k)$  with large  $k$  to drop off fast. In practice, this means we will only keep  $\mathcal{O}(kr)$  and  $\mathcal{O}(kz)$  terms in our analysis. In Fourier space,

the vacuum condition ( $\nabla \times \delta \mathbf{B} = 0$ ) gives us,

$$\frac{in}{r} \delta \hat{B}_z = ik \delta \hat{B}_\phi \quad (C2)$$

$$ik \delta \hat{B}_r = \frac{\partial(\delta \hat{B}_z)}{\partial r} \quad (C3)$$

$$\frac{\partial(r \delta \hat{B}_\phi)}{\partial r} = in \delta \hat{B}_r \quad (C4)$$

And  $\nabla \cdot \mathbf{B} = 0$  gives us,

$$\frac{1}{r} \frac{\partial(r \delta \hat{B}_r)}{\partial r} + \frac{in}{r} \delta \hat{B}_\phi + ik \delta \hat{B}_z = 0 \quad (C5)$$

Replacing  $\delta \hat{B}_r$  and  $\delta \hat{B}_\phi$  from Eqs. (C2) and (C3) in Eq. (C5) gives us the Bessel equation,

$$r^2 \frac{\partial^2(\delta \hat{B}_z)}{\partial r^2} + r \frac{\partial(\delta \hat{B}_z)}{\partial r} - (n^2 + k^2 r^2) \delta \hat{B}_z = 0 \quad (C6)$$

There are two solutions to this: the modified Bessel function of the first kind  $I_n(kr)$  and the modified Bessel function of the second kind  $K_n(kr)$ .  $K_n(kr)$  diverges as  $kr \rightarrow 0$  which is not physical. So, the general solution will only have  $I_n(kr)$  with an arbitrary constant factor. We choose factor to be  $-2\pi \cdot B_0 \alpha(n, k)$ . The  $-2\pi B_0$  constant is added for ease of calculations. This gives us,

$$\delta \hat{B}_z = -2\pi B_0 \alpha(n, k) I_n(kr) \quad (C7)$$

$$\implies \delta B_z = B_0 \int \int \alpha(n, k) I_n(kr) e^{in\phi + kz} dn dk \quad (C8)$$

Now, we require all solutions to fulfill  $B_z(\phi) = B_z(2\pi + \phi)$ . This means  $n$  must be integer numbers. Furthermore, changing the sign of  $n$  leaves Eq. (C6) unchanged, so the solutions must be identical with the change of sign in  $n$ . Given that  $I_{-n}(kr) = I_n(kr)$ , we require  $\alpha(n, k) = \alpha(-n, k) \equiv \alpha_n(k)$ . The general solution to Eq. (C6) in Fourier space will be a superposition of these solutions. After doing a reverse Fourier transform to real space, we thus get,

$$\delta B_z = \sum_{n=0}^{\infty} \delta B_z^{(n)} \quad (C9)$$

$$\delta B_z^{(0)} = -B_0 \int \alpha_0(k) I_0(kr) e^{ikz} dk \quad (C10)$$

$$\delta B_z^{(n)} \equiv -2B_0 \cos(n\phi) \int \alpha_n(k) I_n(kr) e^{ikz} dk \quad (C11)$$

In the long wave approximation, we are only interested in terms of order  $\mathcal{O}(kr)$  and  $\mathcal{O}(kz)$ . This means  $\alpha(k)$  terms drop off fast for higher  $k$  values.  $I_n(kr) \sim \mathcal{O}(k^n r^n)$  so we can ignore modes except  $n = 0$  and  $n = 1$ .

We first focus on  $n = 0$  terms. Integrating  $z$  on both sides Eqs. (C2) and (C3) in real space gives us  $\delta B_\phi^{(0)}$  and  $\delta B_r^{(0)}$ . We require our vector fields to be real. Expanding

up to the first order of  $k$ , we get,

$$\delta B_r^{(0)} = iB_0 \int \alpha_0(k) I_1(kr) e^{ikz} dk \approx \frac{B_0 \mu r}{2} \quad (C12)$$

$$\delta B_z^{(0)} = -B_0 \int \alpha_0(k) I_0(kr) e^{ikz} dk \approx -B_0(\nu + 2\mu z) \quad (C13)$$

Where we have defined,

$$\mu = \frac{i}{2} \int \alpha_0(k) k dk, \quad \nu = \int \alpha_0(k) dk \quad (C14)$$

$\delta B_\phi^{(0)} = 0$  so it can be ignored. We add  $\mathbf{B}^{(0)}$  to hill's vortex.

$$\delta B_r = B_0 \frac{rz}{z_s^2} + B_0 \mu r \quad (C15)$$

$$\delta B_z = B_0 \left( 1 - \frac{2r^2}{r_s^2} - \frac{z^2}{z_s^2} \right) - B_0(\nu + 2\mu z) \quad (C16)$$

We will ignore  $\mu^2$  terms as that is of order  $k^2$ . After some calculations, we can show that,

$$\delta B_r = B_0' \frac{rz'}{z_{s,n}^2}, \quad \delta B_z = B_0' \left( 1 - \frac{2r^2}{r_s'^2} - \frac{z'^2}{z_s'^2} \right) \quad (C17)$$

$$\text{Where, } z' \equiv z + \mu z_s^2, \quad B_0' \equiv B_0(1 - \nu),$$

$$r_s' \equiv r_s \sqrt{1 - \nu}, \quad z_s' \equiv z_s \sqrt{1 - \nu} \quad (C18)$$

Redefining variables completely absorbs the effects in the hill's vortex terms. The effects are merely scaling and coordinate shifts, so such redefinition keeps the topology unchanged. The impact from the redefinition of constants and co-ordinate shift in  $z$  direction in the  $\delta \mathbf{B}^{(1)}$  terms can be absorbed by a redefinition of  $\alpha_1 \rightarrow \alpha_1' = \alpha_1 \exp(-ik\mu z_s^2)/(1 - \nu)$ . So,  $\delta \mathbf{B}^{(0)}$  terms have no impact on the topology of the structure and simply rescale the system. So, we will drop the prime superscript and continue to use the variables as they were.

Now, we focus on the  $n = 1$  term  $\delta \mathbf{B}_z^{(1)}$ . As before, integrating  $z$  on both sides Eqs. (C2) and (C3) in real space gives us  $\delta B_\phi^{(1)}$  and  $\delta B_r^{(1)}$ . We split the solutions into even and odd parity terms.

$$\alpha_1(k) = \alpha_-(k) + i\alpha_+(k) \quad (C19)$$

Here by definition,

$$\alpha_\pm(-k) = \pm \alpha_\pm(k) \quad (C20)$$

This splits the solution into  $\delta \mathbf{B}^{(1)} = \delta \mathbf{B}^{(+)} + \delta \mathbf{B}^{(-)}$  terms where the even parity part is,

$$\delta B_r^{(+)} = -2B_0 \cos \phi \times \int \alpha_+(k) \left( I_0(kr) - \frac{I_1(kr)}{kr} \right) \cos(kz) dk \quad (C21)$$

$$\delta B_\phi^{(+)} = 2B_0 \sin \phi \int \alpha_+(k) \frac{I_1(kr)}{kr} \cos(kz) dk \quad (C22)$$

$$\delta B_z^{(+)} = 2B_0 \cos \phi \int \alpha_+(k) I_1(kr) \sin(kz) dk \quad (C23)$$

The even parity terms completely open up field lines as proven in [23]. We have thus isolated parts of a general perturbation that destroys closure. We require this part to  $\alpha_+(k) = 0$ . What remains is the odd parity part, which is

$$\delta B_r^{(-)} = -2B_0 \cos \phi \times \int \alpha_-(k) \left( I_0(kr) - \frac{I_1(kr)}{kr} \right) \sin(kz) dk \quad (\text{C24})$$

$$\delta B_\phi^{(-)} = 2B_0 \sin \phi \int \alpha_-(k) \frac{I_1(kr)}{kr} \sin(kz) dk \quad (\text{C25})$$

$$\delta B_z^{(-)} = -2B_0 \cos \phi \int \alpha_-(k) I_1(kr) \cos(kz) dk. \quad (\text{C26})$$

Only the  $n = 1$  odd parity perturbations remain in the general perturbation so far, so  $\delta \mathbf{B} = \delta \mathbf{B}^{(-)}$ . Now, we expand the odd parity terms to the first order in  $k$  as required from long wave approximation.

$$\delta \mathbf{B} = -\langle \alpha \rangle \langle k \rangle B_0 (z \cos \phi, -z \sin \phi, r \cos \phi) \quad (\text{C27})$$

where we have defined,

$$\langle \alpha \rangle \equiv \int \alpha_-(k) dk, \quad \langle k \rangle \equiv \frac{1}{\langle \alpha \rangle} \int \alpha_-(k) k dk \quad (\text{C28})$$

Eq. (3) has effectively the same form as Eq. (3) with  $\alpha k$  replaced with  $\langle \alpha \rangle \langle k \rangle$ . So, in summary, the  $n = 0$  type perturbation only rescales the Hill's vortex, and  $n = 1$  type closure preserving perturbations can be reduced to the same form as (3). This proves the claim that our analysis applies to any slow-varying perturbation that preserves closure, which justifies claim 1. ■

#### Appendix D: Validity of the Vortex Model

The unperturbed vortex model used in this paper assumed non-zero vorticity (or current in FRC vortices)  $\propto r$  everywhere. This is valid within the unperturbed separatrix  $r^2/r_s^2 + z^2/z_s^2 = 1$  but not outside. There is nothing mathematically wrong with such a system, but physically it may not be immediately sensible. For example, in case of FRC, current drops to zero as one moves away from FRC core. A more realistic vortex in fluids thus can be modeled as a vortex with non-zero vorticity  $\propto r$  inside the unperturbed separatrix and then dropping to 0 within a layer of thickness  $\sigma$  as was done in [22]. In a perturbed vortex, closed field lines, our primary interest, may exist outside of the unperturbed separatrix, where the model has some error. However, if the error is on the order of  $\alpha B_0 \cdot \mathcal{O}(k^2 r_s^2 + k^2 z_s^2)$ , the topological conclusions from the model remains physically consistent and valid as the error of that order is already ignored.

**Claim:** For  $0 < \alpha \lesssim \alpha_{safe} \equiv \sigma_{min}/r_s \cdot (r_{min}/r_{max})^2$ , the topological conclusions about compact flux surfaces and closed field lines are valid in our vortex model. They fully break down at  $\alpha \sim \alpha_{max} \equiv \alpha_{safe}/(kr_{max})$ .

Here,  $r_{max} \equiv \max(r_s, z_s)$ ,  $r_{min} \equiv \min(r_s, z_s)$ ,  $\sigma_{min} \equiv \min(\sigma, r_s, z_s)$ .

In real-life vortices,  $\sigma/r_s$  is small but non zero. At the extreme end,  $\sigma/r_s$  can go up to 1 or even higher in FRC vortices which were studied in [29, 30]. Thus, the perturbation can be pretty large without impacting the topology inside the separatrix.

**Proof of Claim:** We modeled the unperturbed vortex by Eq. (1).

There is an implicit assumption in the model, the current density (or vorticity) is present everywhere. After some calculation, one can show that,

$$\mathbf{J} = \frac{B_0}{\mu_0} \left( \frac{4}{z_s^2} + \frac{1}{r_s^2} \right) \cdot r \hat{\phi} \quad (\text{D1})$$

This means that the current density keeps increasing all the way to infinity, which is not realistic. In a realistic vortex, the current density goes to 0 outside the separatrix. Thus, outside of the separatrix, the vector fields have a different set of equations than the model we are using. The perturbation we used in Eq. (3) slightly pushes the new outer separatrix by  $\Delta r \sim \alpha k (r_s^2 + z_s^2)/3$  as can be seen [24] and from Eq. (15). Roughly within this distance from the unperturbed separatrix  $r^2/r_s^2 + z^2/z_s^2 = 1$ , the new separatrix does not overlap, and hence, conclusions about closure and topology may not hold. Thus, the vector field has an ambiguous error from using the previous model. If the error is very small compared to the vector field we use in our model, the conclusions in this paper remain valid. We parametrize the elliptical separatrix and its immediate neighborhood with the parametric equation,

$$r = \xi \sin \theta, \quad z = \frac{z_s}{r_s} \xi \cos \theta \quad (\text{D2})$$

For any ellipse,  $\xi$  remains constant and thus can be used as a natural coordinate that respects the boundary condition imposed at  $\xi = r_s$  ellipse. We also define  $\Delta \xi \equiv \xi - r_s$  as roughly a measure of the distance of an ellipse  $\xi$  from the unperturbed separatrix. We now describe a more realistic model for zero helicity vortex where the current falls off to 0 at the edge with thickness  $\sigma \ll r_s$  thickness [22].

$$\nabla \times \mathbf{B}'_0 = \mu_0 \mathbf{J}', \quad (\text{D3})$$

$$\mathbf{J}' = J_0 \sin \theta \cdot \hat{\phi} \begin{cases} \xi/r_s, & \text{if } \xi < r_s \\ 1 - \frac{\Delta \xi}{\sigma} & \text{if } r_s < \xi < r_s + \sigma \\ 0 & \text{if } r_s + \sigma < \xi \end{cases} \quad (\text{D4})$$

In the effective model we used in our analysis, we assumed that there is a non-vanishing current proportional to  $r$  everywhere. In that model we have,

$$\nabla \times \mathbf{B}_0 = \mu_0 \mathbf{J}_0 \quad (\text{D5})$$

$$\mathbf{J}_0 = J \sin \theta \frac{\xi}{r_s} = J_0 \sin \theta \left( 1 + \frac{\Delta \xi}{r_s} \right) \hat{\phi} \quad (\text{D6})$$

Thus, in the  $r_s < \xi < r_s + \sigma$  region, we get an error of  $\Delta \mathbf{B} \equiv \mathbf{B}'_0 - \mathbf{B}_0$ . This error fulfills,

$$\nabla \times \Delta \mathbf{B} = \mu_0 J_0 \sin \theta \left( \frac{1}{r_s} + \frac{1}{\sigma} \right) \Delta \xi \hat{\phi} \quad (\text{D7})$$

and the boundary condition,

$$\Delta \mathbf{B}(r_s, \theta, \phi) = 0 \quad (\text{D8})$$

$$\implies \frac{\partial}{\partial \theta} \Delta \mathbf{B}(r_s, \theta, \phi) = \frac{\partial}{\partial \phi} \Delta \mathbf{B}(r_s, \theta, \phi) = 0 \quad (\text{D9})$$

We will express the vector field into components  $(\Delta B_\xi, \Delta B_\theta, \Delta B_\phi)$ . The system is symmetric for  $\phi$  and hence  $\partial_\phi \rightarrow 0$ . There is no error current in  $\xi$  and  $\theta$  components.

$$(\nabla \times \Delta \mathbf{B})_\xi = 0, \quad (\nabla \times \Delta \mathbf{B})_\theta = 0 \quad (\text{D10})$$

$$\implies \frac{\partial}{\partial \theta} (\Delta B_\phi \sin \theta) = 0, \quad -\frac{\partial}{\partial \xi} (\xi \Delta B_\phi) = 0 \quad (\text{D11})$$

$$\implies \Delta B_\phi = \frac{C}{\xi \sin \theta} \quad (\text{D12})$$

From Eq. (D8),  $\Delta B_\phi(r_s, \theta, \phi) = 0$  which gives us  $C = 0$ . Thus we have

$$\Delta B_\phi = 0, \quad \text{everywhere} \quad (\text{D13})$$

$$\implies \frac{\partial}{\partial \xi} \Delta B_\phi = 0 \quad (\text{D14})$$

The  $\theta$  component of  $\Delta \mathbf{B}$  can be analyzed via the curl of the  $\phi$  component, and the  $\xi$  component can be analyzed via the divergence. At  $\xi = r_s$  surface,  $\Delta \xi = 0$  so,

$$\nabla \times \Delta \mathbf{B}|_{\xi=r_s} = \mathbf{0} \quad (\text{D15})$$

$\phi$  component gives us,

$$\left( \frac{\partial \Delta B_\theta}{\partial \xi} + \frac{\Delta B_\theta}{\xi} - \frac{\partial_\theta \Delta B_\xi}{\xi \sqrt{\sin^2 \theta + z_s^2/r_s^2 \cdot \cos^2 \theta}} \right) \Big|_{\xi=r_s} = 0 \quad (\text{D16})$$

Given that  $\Delta B_\phi = 0$  the divergence condition  $\nabla \cdot \Delta \mathbf{B} = 0$  becomes,

$$\left( \frac{\partial \Delta B_\xi}{\partial \xi} + \frac{\Delta B_\xi}{\xi} + \frac{\partial_\theta \Delta B_\theta}{\xi \sqrt{\sin^2 \theta + z_s^2/r_s^2 \cdot \cos^2 \theta}} \right) \Big|_{\xi=r_s} = 0 \quad (\text{D17})$$

Using Eqs. (D8) and (D9) we can reduce Eqs. (D17) and (D16) to,

$$\frac{\partial}{\partial \xi} \Delta B_\theta \Big|_{\xi=r_s} = 0, \quad \frac{\partial}{\partial \xi} \Delta B_\xi \Big|_{\xi=r_s} = 0 \quad (\text{D18})$$

Summarizing Eqs. (D14) and (D18) we can write,

$$\frac{\partial}{\partial \xi} \Delta \mathbf{B} \Big|_{\xi=r_s} = \mathbf{0} \quad (\text{D19})$$

Given Eqs. (D8) and (D19), after a Taylor expansion upto first order, we can show

$$\Delta \mathbf{B}(r_s + \Delta \xi, \theta, \phi) = \mathbf{0} + \mathcal{O}(\Delta \xi^2) \quad (\text{D20})$$

So, the magnitude of error  $\Delta B \equiv |\Delta \mathbf{B}(r_s + \Delta \xi, \theta, \phi)|$  is 0 up to first order in  $\Delta \xi$ . Upto the second order, we need to compare it to the dimensioned forms available. The error will be dominated by the smallest length scale  $\sigma_{min}$ . Thus,

$$\Delta B \sim \frac{\mu_0 J_0 \Delta \xi^2}{\sigma_{min}} \quad (\text{D21})$$

We compare this with the vector field in either model to get an error ratio. We know from Eqs. (D4) and (D1) that current on the separatrix is  $J_0$  where,

$$J_0 = \frac{B_0 r_s}{\mu_0} \left( \frac{4}{z_s^2} + \frac{1}{r_s^2} \right) \sim \frac{B_0 r_s}{\mu_0 r_{min}^2} \quad (\text{D22})$$

$$\implies \Delta B \sim \frac{B_0 \Delta \xi^2 r_s}{r_{min}^2 \sigma_{min}} \quad (\text{D23})$$

Ignoring vector fields of order  $\alpha B_0 k^2 (r_s^2 + z_s^2) \sim \alpha B_0 k^2 r_{max}^2$  is already consistent with our analysis. So the largest  $\Delta \xi$ , which we label as safe length, that does not have a significant error on our analysis, is,

$$\frac{B_0 \Delta \xi^2 r_s}{r_{min}^2 \sigma_{min}} \sim \alpha B_0 k^2 r_{max}^2 \quad (\text{D24})$$

$$\implies \Delta \xi_{safe} \sim \sqrt{\frac{\alpha k^2 r_{max}^2 r_{min}^2 \sigma_{min}}{r_s}} \quad (\text{D25})$$

The theory breaks down when the error is of order equal to the perturbation which is  $\alpha B_0 k (r_s + z_s) \sim \alpha B_0 k r_{max}$ .

$$\frac{B_0 \Delta \xi^2 r_s}{r_{min}^2 \sigma_{min}} \sim \alpha B_0 k r_{max} \quad (\text{D26})$$

$$\implies \Delta \xi_{max} \sim \sqrt{\frac{\alpha k r_{max} r_{min}^2 \sigma_{min}}{r_s}} \quad (\text{D27})$$

The central topological effects, such as closure and compact flux surfaces, happen inside the new perturbed separatrix. Its center shifts from the unperturbed separatrix by  $\alpha k (r_s^2 + z_s^2)/3$ , and it has a radius of  $\sim r_s$ . So the largest deviation  $\Delta \xi$  we need to worry about in the new separatrix is

$$\Delta \xi_{crit} \sim \alpha k \frac{r_s^2 + z_s^2}{3} \sim \alpha k r_{max}^2 \quad (\text{D28})$$

The topological conclusion remains unaffected when  $\Delta \xi_{crit}$  is well within or comparable to the safety region.

$$\Delta \xi_{crit} \sim \Delta \xi_{safe} \quad (\text{D29})$$

And the theory will break down when the breakdown error length is comparable to the cutoff length,

$$\Delta \xi_{crit} \sim \Delta \xi_{max} \quad (\text{D30})$$

After straightforward calculations, these conditions reduce to,

$$\alpha_{safe} \sim \frac{\sigma_{min}}{r_s} \left( \frac{r_{min}}{r_{max}} \right)^2 \quad (D31)$$

$$\alpha_{max} \sim \frac{1}{kr_{max}} \frac{\sigma_{min}}{r_s} \left( \frac{r_{min}}{r_{max}} \right)^2 = \frac{\alpha_{safe}}{kr_{max}} \quad (D32)$$

Even though  $\sigma/r_s$  is small, the breakdown limit of the perturbation can be relatively larger as  $kr_{max}$  can be comparable or even smaller than that. ■

- 
- [1] P. Bellan. *Spheromaks*. Imperial Coplege Press, 2000.
- [2] Loren C. Steinhauer. Review of field-reversed configurations. *Physics of Plasmas*, 18(7):070501, 2011.
- [3] Michael Paluszek, Annie Price, Zoe Koniaris, Christopher Galea, Stephanie Thomas, Samuel Cohen, and Rachel Stutz. Nuclear fusion powered titan aircraft. *Acta Astronautica*, 210:82–94, 2023.
- [4] S.A. Cohen and R.D. Milroy. Maintaining the closed magnetic-field-line topology of a field-reversed configuration with the addition of static transverse magnetic fields. *Physics of Plasmas*, 7:2539–2545, 2000.
- [5] S.A. Cohen and A.H. Glasser. Ion heating in the field-reversed configuration by rotating magnetic fields near the ion-cyclotron resonance. *Physical Review Letters*, 85:5114, 2000.
- [6] A.H. Glasser and S.A. Cohen. Ion and electron acceleration in the field-reversed configuration with an odd-parity rotating magnetic field. *Physics of Plasmas*, 9(5):2093–2102, 2002.
- [7] S. Solov'ev. The theory of hydromagnetic stability in toroidal plasmas. *Sov. Phys. JETP*, 26:400, 1968.
- [8] M.J. Hill. On a spherical vortex. *Phil. Trans. Roy. Soc. A*, 185, 1894.
- [9] P. Barge and J. Sommeria. Did planet formation begin inside persistent gaseous vortices? *Astronomy & Astrophysics*, 295:L1–L4, 1995.
- [10] R. V. E. Lovelace, H. Li, S. A. Colgate, and A. F. Nelson. Rossby wave instability of Keplerian accretion disks. *The Astrophysical Journal*, 513(2):805–810, 1999.
- [11] H. Meheut, C. Yu, and D. Lai. On the survival and non-linear evolution of vortices in discs: 3d linear analysis. *Monthly Notices of the Royal Astronomical Society*, 422(3):2399–2410, 2012.
- [12] H. K. Moffatt. Vorticity, vortex dynamics and rotating flows. *Journal of Fluid Mechanics*, 432:1–20, 1991.
- [13] John O. Dabiri. Optimal vortex formation as a unifying principle in biological propulsion. *Annual Review of Fluid Mechanics*, 42:265–282, 2010.
- [14] H. Rosett and M. Gharib. Vortex formation in biological flows: From hearts to jellyfish. *Physics of Fluids*, 31:081301, 2019.
- [15] Shawn C. Shadden, John O. Dabiri, and Jerrold E. Marsden. Lagrangian analysis of fluid transport in empirical vortex ring flows. *Physics of Fluids*, 18(4):047105, 2006.
- [16] Yieh-Hei Wan. Variational principles for Hill's spherical vortex and nearly spherical vortices. *Transactions of the American Mathematical Society*, 308(1):299–312, 1988.
- [17] Charles J. Amick and Leib Fraenkel. The uniqueness of Hill's spherical vortex. *Archive for Rational Mechanics and Analysis*, 99(1):191–208, 1987.
- [18] J. Wesson. *Tokamaks, 4th ed.* Oxford University Press, 2011.
- [19] Patrick W. Keller and Alexei F. Cheviakov. On the Hill's spherical vortex in fluid and plasma, its generalization, and stability. *Journal of Fluid Mechanics*, 939:A18, 2022.
- [20] H. K. Moffatt and D. W. Moore. The response of Hill's spherical vortex to a small axisymmetric disturbance. *Journal of Fluid Mechanics*, 87:749–760, 1978.
- [21] Kyudong Choi. Stability of Hill's spherical vortex. *arXiv preprint arXiv:2011.06808*, 2020.
- [22] P. Orlandi. The three-dimensional instabilities and destruction of the Hill's vortex. *arXiv preprint arXiv:2004.14416*, 2020.
- [23] A. H. Boozer. Magnetic surfaces in the reversed-field geometry. *Nuclear Fusion*, 18:1663, 1978.
- [24] T. Ahsan and S.A. Cohen. An analytical approach to evaluating magnetic-field closure and topological changes in FRC devices. *Physics of Plasmas*, 29:4850, 2022.
- [25] Henri Poincaré. On curves defined by differential equations. *Journal de Mathématiques Pures et Appliquées*, 8:251–296, 1892.
- [26] H. Hopf. Vektorfelder in n-dimensionalen mannigfaltigkeiten. *Mathematische Annalen*, 96:209–221, 1926.
- [27] A. H. Glasser and S. A. Cohen. Ion and electron acceleration in the field-reversed configuration with an odd-parity rotating magnetic field. *Physics of Plasmas*, 9:2093, 2002.
- [28] A.H. Glasser and S.A. Cohen. Simulating single-particle dynamics in magnetized plasmas: The RMF code. *Review of Scientific Instruments*, 62:4850, 2022.
- [29] H. Gota, M. Tuszewski, E. Trask, E. Garate, M. W. Binderbauer, T. Tajima, L. Schmitz, B. H. Deng, H. Y. Guo, S. Aefsky, et al. Improved confinement of C-2 field-reversed configuration plasmas. *Fusion Science and Technology*, 68(1):44–49, 2015.
- [30] L. C. Steinhauer, T. Roche, and J. D. Steinhauer. Anatomy of a field-reversed configuration. *Physics of Plasmas*, 27(11):112508, 2020.